$$+\frac{1}{2N}\Big)+m^2\Big[\frac{F}{2}+\frac{3FB}{N^2}-\frac{F}{N^2}+\frac{FB}{N}+\frac{3F}{2N}+\frac{7F^2}{2N^2}+\frac{F^2}{2N}+\frac{8}{F}+\frac{12B}{FN}+\frac{16}{FN}$$

$$-\frac{1}{4}+\frac{B}{2}+\frac{N}{4}-\frac{B^2}{2N^2}-\frac{B}{N^2}-\frac{1}{2N^2}+\frac{B^2}{2N}-\frac{3B}{2N}+\frac{5}{N}+T\Big(\frac{4B}{FN}-\frac{3F}{N^2}-\frac{F}{N}+\frac{12}{FN}$$

$$+\frac{4}{F^2}-\frac{1}{2}+\frac{B}{N^2}+\frac{9}{N^2}-\frac{B}{N}-\frac{5}{2N}\Big)-\frac{T^2}{N}\Big(\frac{2}{F}+\frac{1}{2N}-\frac{1}{2}\Big)\Big]\Big\}+1+\frac{B^2}{N^2}-\frac{B}{N^2}-\frac{3}{N^2}$$

$$+\frac{B}{N}+\frac{4}{N}-\frac{4}{F^2}-\frac{8}{FN}+\frac{F^2}{N^2}+\frac{2FB}{N^2}+\frac{T}{N}\Big(1+\frac{1}{N}\Big)+m^2\Big[\frac{2}{F}-\frac{5F}{N^2}-\frac{F}{N}+\frac{4B}{FN}+\frac{8}{FN}$$

$$+\frac{4}{F^2}-1-\frac{3B}{N^2}+\frac{5}{N^2}-\frac{B}{N}-\frac{T}{N}\Big(\frac{4}{F}+\frac{1}{N}-1\Big)\Big]+\frac{S}{N}\Big\{\frac{1}{2N}+\frac{1}{2}+m^2\Big(\frac{1}{2N}+\frac{1}{2}-\frac{2}{F}\Big)\Big\}.$$

---

*Work supported in part by the U. S. Atomic Energy Commission under Contract No. AT(30-1)-3668B.

[1]E. A. Choban, Yadern. Fiz. 7, 375 (1968); 9, 392 (1969) [Soviet J. Nucl. Phys. 7, 245 (1968); 9, 230 (1969)].

[2]F. A. Berends and G. B. West, Phys. Rev. D 1, 122 (1970); 2, 1354 (1970).

[3]We use the metric and conventions of J. D. Bjorken and S. D. Drell, *Relativistic Quantum Fields* (McGraw-Hill, New York, 1965). In particular, $\hbar=c=1$, $\alpha=e^2/4\pi$. Note that there is an over-all sign error in their Lagrangian for spin-1 electrodynamics. The effect of κ (the anomalous magnetic moment of the W in units of $e/2M_W$) is incorporated following T. D. Lee and C. N. Yang, Phys. Rev. 128, 885 (1962).

[4]R. W. Brown and J. Smith, Phys. Rev. D 3, 207 (1971).

PHYSICAL REVIEW D VOLUME 4, NUMBER 3 1 AUGUST 1971

Intermediate Boson. II. Theoretical Muon Spectra in High-Energy Neutrino Experiments*

R. W. Brown
Brookhaven National Laboratory, Upton, New York 11973
and Case Western Reserve University,† Cleveland, Ohio 44106

and

R. H. Hobbs
Laboratory for Nuclear Science and Department of Physics, Massachusetts Institute of Technology, Cambridge, Massachusetts 02139

and

J. Smith
The Institute for Theoretical Physics, State University of New York at Stony Brook, Stony Brook, New York 11790

(Received 17 February 1971)

We present here the theoretical angular and energy distributions for the W boson, the "prompt" muon, and the decay muon in the reaction $\nu+Z\to Z+W+\mu$ with the subsequent fast decay $W\to\mu+\nu$. A discussion of the W's polarization is included. In particular, the deep-inelastic contributions to the incoherent production mode and the effect of the W's anomalous magnetic moment are considered. Our emphasis is on the energies available at the National Accelerator Laboratory and corresponding attainable W-boson masses.

I. INTRODUCTION

This is the second in a series of three papers dealing with the possibility that the W boson may be found at the National Accelerator Laboratory (N.A.L.). The first paper,[1] which we refer to as I, contains the total production cross sections for the reactions

$$\nu_\mu+Z\to\mu^-+W^++Z' \tag{1.1}$$

and

$$\mu^+ + Z \to \bar{\nu}_\mu + W^+ + Z'. \tag{1.2}$$

Here we consider the theoretical angular and energy spectra in (1.1) of the W^+, the μ^- (the "prompt muon"), and the μ^+ (the decay muon) from the fast semiweak decay

$$W^+ \to \mu^+ + \nu_\mu. \tag{1.3}$$

Since it has been shown[1-4] that (1.1) is much more probable than (1.2), we do not address ourselves to the muon-induced reaction. There are some recent results[4] available, however, for the W polarization pertaining to reaction (1.2).

The third and final paper deals with the differences between the four-fermion predictions[5] and the virtual W-boson predictions for the reaction

$$\nu_\mu + Z \to \mu^- + \mu^+ + \nu_\mu + Z'. \tag{1.4}$$

In the W-boson theory, this reaction would go by way of a virtual W decay, and may give us an indication of the W's existence even in the event that it is too heavy to actually be produced.

Our motivation for calculating the muon spectra is primarily an experimental one. We need to understand how to separate the W-boson signal from the background noise. Furthermore, an understanding of the W-boson's spectra and polarization is also important in the event that its dominant decay involves hadrons instead of the $\mu\nu$ pair in (1.3). As evidence of the usefulness of such calculations, there has recently appeared[6] an engaging suggestion for distinguishing the W's decay hadrons from the deep-inelastic events based partly on the results of this paper.

The previous discussions of muon and W spectra and W polarization in (1.1) have been limited to lower beam energies ($E_\nu \leq 10$ GeV) with a typical boson mass, M_W, on the order of the proton mass, M_p. Lee, Markstein, and Yang[7] a decade ago considered the prompt-muon energy distribution in reaction (1.1), finding the expected low-energy peak (corresponding to the W taking most of the energy). Later, Bell and Veltman[8] calculated the average polarization of the W for a copper target in the same reaction. They found it to be predominantly left handed and gave the associated decay-muon angular distribution. Using a covariant Weizsäcker-Williams approximation, Überall[9] computed angular and energy distributions for both the muon and the W in reaction (1.1) and, furthermore, for the decay muon in reaction (1.2). This last reference included a study of the polarization of the W.

Our work presented here is, in part, a repeat of the numerical calculations performed by Lee *et al.*[7] and Bell and Veltman,[8] but is done for higher energies. Going beyond what has been considered before, we present the W spectra and the decay angular distribution without recourse to approximations, such as in the Weizsäcker-Williams approach. Moreover, an estimate of the spectra pertaining to the deep-inelastic channels is also given here. The details of our kinematical analysis have been included since we feel that they are useful in understanding our results. The previous work has been, for the most part, presentations of results only.

The outline of our paper is as follows. The kinematical notation is defined and the general differential cross section is written down in Sec. II. The angular and energy distributions of the prompt μ^- are discussed in Sec. III while those for the W^+ are discussed in Sec. IV. The W's average polarization is described next in Sec. V. Section VI contains the results from an explicit evaluation of the decay-muon angular distribution. Effects of the inclusion of deep-inelastic W production are given in Sec. VII. Finally, discussions and conclusions comprise Sec. VIII.

II. DIFFERENTIAL CROSS SECTION

We assume that perturbation theory, to lowest order in the electromagnetic and semiweak couplings, is quantitatively reliable. The lowest-order matrix element for reaction (1.1) and our notation[10] for the four-momenta are illustrated by way of Feynman diagrams in Fig. 1. Although our preliminary remarks here have been given before in I, it is worthwhile repeating some of them.

Our laboratory frame notation for a proton target at rest is

$$\begin{aligned} k_1^2 &= E_1^2 - \vec{k}_1^2 = 0, \\ k_2^2 &= E_2^2 - \vec{k}_2^2 = \mu^2, \\ k^2 &= E_k^2 - \vec{k}^2 = M_W^2, \\ p_1^2 &= E_{p_1}^2 - \vec{p}_1^2 = M_p^2. \end{aligned} \tag{2.1}$$

The masses μ, M_W, and M_p are those of the muon, W boson, and proton, respectively. We use units such that $M_W = 1$, and, furthermore, we define

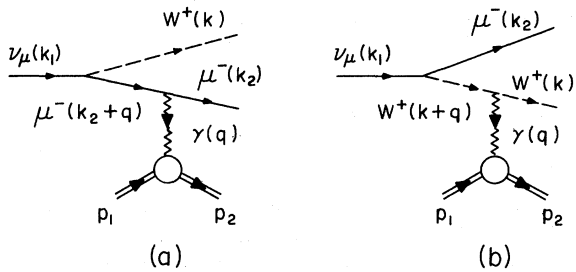

FIG. 1. Feynman diagrams for the reaction (1.1).

$q \equiv p_2 - p_1$ and $p \equiv p_2 + p_1$. The c.m. energy squared and four-momentum transfer squared are, respectively,

$$S = (p_1 + k_1)^2 = 2M_p E_1 + M_p^2, \qquad T = q^2. \tag{2.2}$$

If the final-state spins are left undetected and the target is unpolarized, the differential cross section is[11]

$$d^9\sigma = \frac{1}{32\pi^3} \frac{\alpha^2 g_W^2}{E_1 M_p} \frac{d^3k_2}{E_2} \frac{d^3k}{E_k} \frac{d^3p_2}{E_{p_2}} \delta^4(k_1 - q - k_2 - k)\mathfrak{F}\,. \tag{2.3}$$

Here

$$\mathfrak{F} \equiv T^{-2} P_{\nu\mu} K_{\beta\alpha} L^{\beta\nu\mu\alpha} \tag{2.4}$$

in terms of the proton trace (and hence the proton electric and magnetic form factors),

$$P_{\nu\mu} = (T g_{\nu\mu} - q_\nu q_\mu) G_1 + p_\nu p_\mu G_2, \qquad G_1 \equiv G_M^2(T), \quad G_2 \equiv [G_E^2(T) + \tau G_M^2(T)]/(1+\tau), \quad \tau \equiv -T/4M_p^2, \tag{2.5}$$

the W polarization sum

$$K_{\beta\alpha} = -g_{\beta\alpha} + k_\beta k_\alpha, \tag{2.6}$$

and the lepton trace

$$\begin{aligned} L^{\beta\nu\mu\alpha} = \mathrm{Tr}\{ & \not{k}_1(1+\gamma_5)\{\gamma^\beta(\not{q}\gamma^\nu + 2k_2^\nu)F^{-1} - [\gamma^\beta(2k+q)^\nu + (1+\kappa)(\not{q}g^{\beta\nu} - q^\beta\gamma^\nu) \\ & + \mu(1-\kappa)(q^\beta k^\nu - k\cdot q g^{\beta\nu}) + \mu\kappa(T g^{\beta\nu} - q^\beta q^\nu)]B^{-1}\}(\not{k}_2 + \mu)\{(\gamma^\mu \not{q} + 2k_2^\mu)\gamma^\alpha F^{-1} \\ & - [(2k+q)^\mu\gamma^\alpha + (1+\kappa)(\not{q}g^{\mu\alpha} - \gamma^\mu q^\alpha) + \mu(1-\kappa)(k^\mu q^\alpha - k\cdot q g^{\mu\alpha}) + \mu\kappa(T g^{\mu\alpha} - q^\mu q^\alpha)]B^{-1}\}. \end{aligned} \tag{2.7}$$

The denominators of the fermion and boson propagators have been defined as

$$F \equiv (k_2 + q)^2 - \mu^2 = T + 2k_2\cdot q, \qquad B \equiv (k+q)^2 - 1 = T + 2k\cdot q, \tag{2.8}$$

respectively. The anomalous magnetic moment κ has been included[12] in (2.7).

We have given an explicit expression for $\mathfrak{F}$ in I. Including the initial c.m. energy, it is a function of five independent variables. The familiar dipole fits for the proton and neutron form factors are[13]

$$G_{E,p} \cong \frac{G_{M,p}}{2.79} \cong -\frac{G_{M,n}}{1.91} \cong \left(1 - \frac{T}{0.71\ (\mathrm{GeV}/c)^2}\right)^{-2}, \qquad G_{E,n} \cong 0. \tag{2.9}$$

These serve as input for the incoherent calculations.

We have seen in I that the static nuclear form factors drastically reduce the corresponding coherent cross sections compared to the incoherent cross sections, unless we are very far above threshold. Although this means that we concentrate on incoherent scattering, some coherent calculations have been included here for comparison. In those calculations, we have employed the exponential nuclear form factor[14]

$$F(\vec{q}^2) = Z\exp(-\tfrac{1}{6}\vec{q}^2 a^2), \qquad a = (\tfrac{3}{5})^{1/2}(1.3A^{1/3}) \times 10^{-13}\ \mathrm{cm}, \tag{2.10}$$

where Z is the nuclear charge and A is the atomic number. We have not used the more realistic Fermi form factor since the additional numerical integration could not be quickly handled. As it is, we do four integrations over the differential cross section for the μ^- and W^+ spectra and *six* for the decay angular distributions. However, the total cross section calculated according to our methods

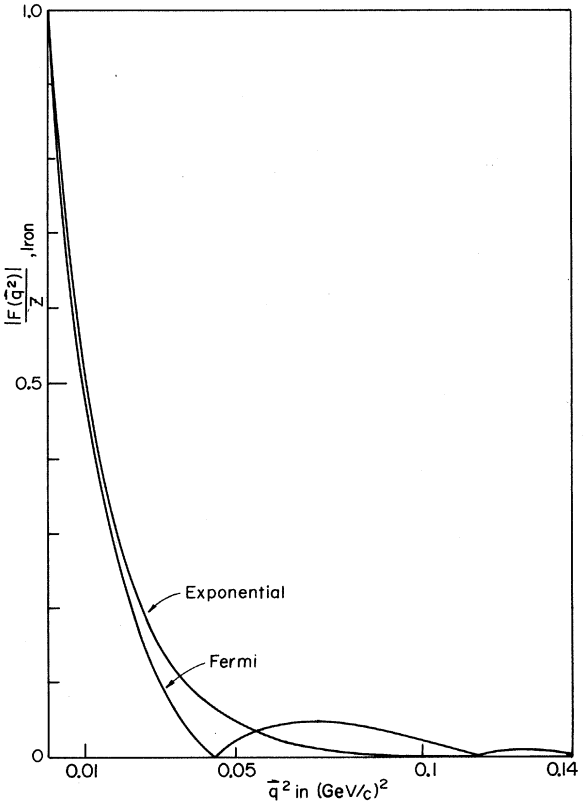

FIG. 2. Nuclear Fermi and exponential form factors for an iron nucleus.

in I using (2.10) is an adequate approximation (about 20% higher) to the corresponding Fermi one for the iron target that we shall consider here, since we take the incident energy to be far above threshold. We give a plot of both of the Fermi and exponential form factors for iron in Fig. 2.

A final remark is that we first wrote programs for the incoherent calculations and then converted these to the coherent case. The conversion was simply a matter of substituting the exponential nuclear form factor (2.10) for G_E and G_M and using the nuclear target mass in place of the nucleon mass. The fact that this corresponds to a Dirac nuclear magnetic moment is unimportant since the moment corrections to coherent scattering are small, even though the moment contributions to incoherent scattering are important.

III. THE PROMPT MUON SPECTRA

We discuss first the energy and angular distributions for the final μ^- in reaction (1.1). The differential cross section in energy for a proton target is, from (2.3),

$$\frac{d\sigma}{dE_2} = \frac{1}{16\pi^2}\frac{\alpha^2 g_W{}^2|\vec{k}_2|}{E_1 M_p}\int_{\cos\theta_{\max}}^{1} d\cos\theta\, I(E_2,\theta),$$
$$I(E_2,\theta)\equiv\int_{\cos\eta_{\max}}^{1} d\cos\eta\int_0^{2\pi} d\chi\sum_{E_{p_2}=E_\pm}\frac{|\vec{p}_2|^2}{|r^0|\vec{p}_2| - |\vec{r}|E_{p_2}\cos\eta|}\mathcal{F}, \tag{3.1}$$

where $r\equiv p_2+k=p_1+k_1-k_2$ and the angles are defined according to Fig. 3. The limits of integration and the two roots $E_\pm$ from the energy δ function (corresponding to two c.m. angles for each laboratory η) are given by

$$\cos\theta_{\max}=\max\left[-1,\frac{(1+M_p)^2+2E_2(E_1+M_p)-S-\mu^2}{2E_1|\vec{k}_2|}\right],$$
$$\cos\eta_{\max}=\frac{[4M_p{}^2r_0{}^2-(r^2+M_p{}^2-1)^2]^{1/2}}{2M_p|\vec{r}|}>0,$$
$$E_\pm=\frac{1}{2(r^2+|\vec{r}|^2\sin^2\eta)}\{r_0(r^2+M_p{}^2-1)\pm|\vec{r}|\cos\eta\,[(r^2+M_p{}^2-1)^2-4M_p{}^2(r^2+|\vec{r}|^2\sin^2\eta)]^{1/2}\}. \tag{3.2}$$

The muon energy range in (3.1) is

$$E_{2\,\min}\le E_2\le E_{2\,\max}, \tag{3.3}$$

where

$$E_{2\,\max}=E_2^+,$$
$$E_{2\,\min}=\begin{cases}E_2^-, & S_{\text{thresh}}\le S\le S_\mu\\ \mu, & S_\mu\le S\end{cases} \tag{3.4}$$

with

$$S_{\text{thresh}}\equiv(1+M_p+\mu)^2,\quad S_\mu\equiv S_{\text{thresh}}+\frac{\mu}{M_p-\mu}(1+\mu)^2,$$
$$E_2^\pm=\frac{1}{2S}\{(E_1+M_p)[S+\mu^2-(M_p+1)^2]\pm E_1\{[S+\mu^2-(M_p+1)^2]^2-4\mu^2S\}^{1/2}\}. \tag{3.5}$$

We address ourselves here to cases sufficiently above threshold so that $E_{2\,\min}=\mu$.

For the differential cross section in angle, we have

$$\frac{d\sigma}{d\cos\theta}=\frac{1}{16\pi^2}\frac{\alpha^2 g_W{}^2}{E_1M_p}\int_{E_{2\,\min}(\theta)}^{E_{2\,\max}(\theta)} dE_2|\vec{k}_2|\,I(E_2,\theta) \tag{3.6}$$

in the notation of Eq. (3.1). Here

$$E_{2\,\max}(\theta)=E_2^+(\theta),$$
$$E_{2\,\min}(\theta)=\begin{cases}E_2^-(\theta), & S_{\text{thresh}}\le S\le S_\mu\\ \mu, & S_\mu\le S\end{cases} \tag{3.7}$$

in which

$$E_2^{\pm}(\theta) = \frac{1}{2(S+E_1^{\,2}\sin^2\theta)}\{(E_1+M_p)[S+\mu^2-(M_p+1)^2] \pm E_1\cos\theta[(S+\mu^2-(M_p+1)^2)^2 - 4\mu^2(S+E_1^{\,2}\sin^2\theta)]^{1/2}\}\,. \quad (3.8)$$

Our range in θ extends from $\theta=0$ out to $\theta=\theta_{\max}$ defined by

$$\sin^2\theta_{\max} = \frac{[S+\mu^2-(M_p+1)^2]^2 - 4\mu^2 S}{4\mu^2 E_1^{\,2}}\,, \qquad S_{\text{thresh}} \le S \le S_\mu \quad (3.9)$$

or $\theta_{\max}=\pi$, $S>S_\mu$. We are always in this latter region.

All three of the integrals in Eqs. (3.1) and (3.6) have been performed by using a Gaussian quadrature numerical integration routine on the Brookhaven CDC 6600 computer. The calculations were checked by integrating (3.1) over E_2 and (3.6) over θ in order to compare the resulting total cross sections with those found using the different approach described in I. In these and later calculations, it was important that the small-angle regions were covered with enough integration points.

The set of beam energies and W-boson masses which is considered in the presentation of incoherent results is

$$\left\{\begin{matrix} M_W = 5 \text{ for } E_1 = 50,\ 100,\ 200 \\ M_W = 10 \text{ for } E_1 = 100,\ 200 \end{matrix}\right\}. \quad (3.10)$$

These incident energies are representative of what we may expect at N.A.L.; the values chosen for M_W span those of interest in view of the present experimental limit[15] $M_W \gtrsim 2$ or 3 GeV/c^2. Only in the situation where $M_W=5$, $E_1=200$ do we have an appreciable coherent contribution, and so the coherent results are given only for that case. Furthermore, we restrict the presentation of contributions from incoherent scattering off neutrons, inelastic channels, and the effects due to changing the magnetic moment, κ, to the same case: $M_W=5$, $E_1=200$. This is sufficiently representative for an adequate illustration of the corresponding changes in the results. These remarks, together with those of the previous paragraph, apply *mutatis mutandis* to Secs. III–VI. For the convenience of the reader, we include in Table I the total cross sections for all of these cases.

The set of $d\sigma/dE_2$ plots for the array (3.10) with $\kappa=0$ (no anomalous magnetic moment) is given in Fig. 4. The target here is the free proton. We see that the negatively charged muons are peaked at very low energies corresponding to the fact that

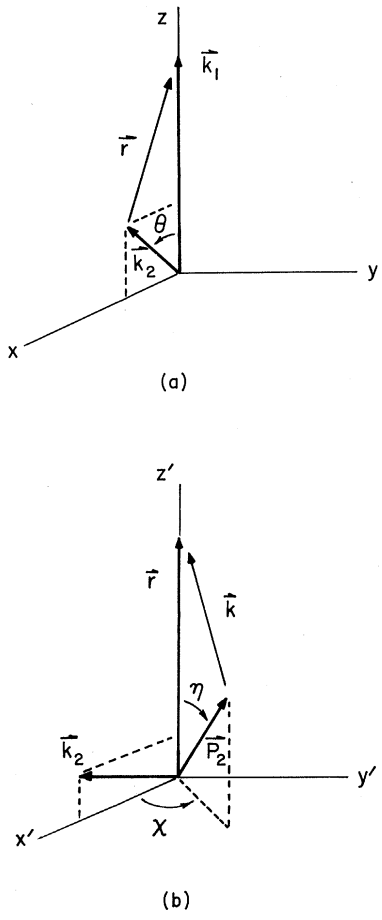

FIG. 3. Coordinate system used in the calculation of the μ^- spectra.

TABLE I. Total cross sections for W-boson production by neutrinos in units of 10^{-38} cm^2 at the mass and energy values considered in this paper. $\sigma(p)$, $\sigma(n)$ refer to scattering off a free proton and a free neutron, respectively. σ_{inel} is calculated using a fit to the inelastic electron scattering form factors as described in the text. σ_c(Fe) refers to the scattering off an iron nucleus with an exponential form factor in momentum space, and is normalized per proton. $\kappa=0$ unless otherwise stated.

M_W (GeV/c^2)	5	5	5	10	10
E_ν (GeV)	50	100	200	100	200
$\sigma(p)$, $\kappa=-1$	...	...	44.9	...	...
$\sigma(p)$, $\kappa=0$	3.05	18.0	50.6	0.0991	4.76
$\sigma(p)$, $\kappa=+1$	...	...	61.5	...	...
$\sigma(n)$	...	...	6.81	...	...
σ_{inel}	...	...	29.0	...	...
σ_c (Fe)/26	...	...	41.7	...	...

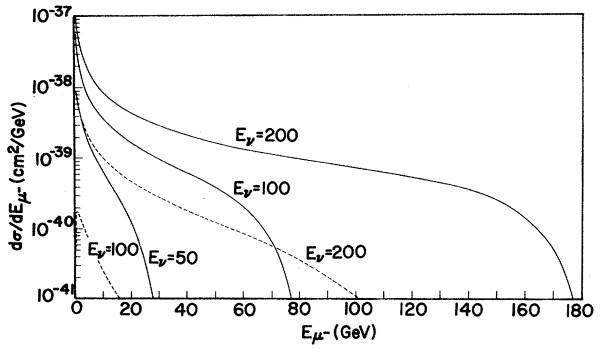

FIG. 4. Plot of $d\sigma/dE_{\mu^-}$ in cm^2/GeV for a free proton. The solid lines are for $M_W = 5$ GeV/c^2, the dashed lines are for $M_W = 10$ GeV/c^2, and $\kappa = 0$.

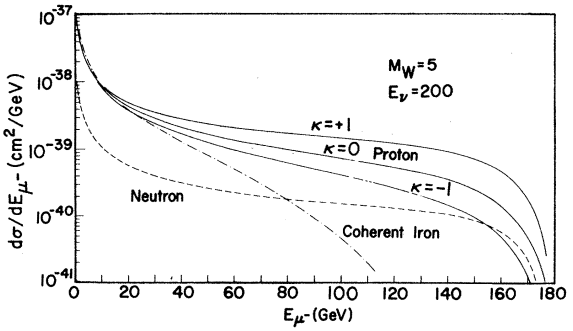

FIG. 6. Plot of $d\sigma/dE_{\mu^-}$ in cm^2/GeV for scattering off a proton target, a neutron target, and an iron nucleus target (normalized per proton). All curves are drawn for $E_\nu = 200$ GeV and $M_W = 5$ GeV/c^2. $\kappa = 0$ unless otherwise stated.

the form factors limit us to small T (and hence small W-μ invariant mass). The ratio of the boson's energy to the muon's energy is given by M_W/μ at minimum $|T|$, and since we are restricted to values of the momentum transfer close to this limit, the μ^- obtains little of the available energy. For an increase in E_1 at a given M_W, the muon obtains more and more of its share of the energy (E_k/E_2 decreases) and the average W-μ invariant mass increases.

A better picture of the prompt muon energy distribution can be obtained by considering Fig. 5. There we have plotted the fraction of the negative muons with energy greater than a given value. The remarks made earlier are perhaps better understood here; the logarithmic scale in Fig. 4 is somewhat misleading.

Using the exponential form factor (2.10) and concentrating on iron ($Z = 26$, $A = 56$) as a typical target, a coherent curve (per proton) analogous to the proton ones described above is plotted in Fig. 6. The difference between the two cases is simply that the exponential form factor limits the T range much more severely. Hence, the average energy of the μ^- is smaller. The $\kappa = \pm 1, 0$ proton and the $\kappa = 0$ neutron results are given also in Fig. 6. The magnetic moment is seen to be a factor only at larger

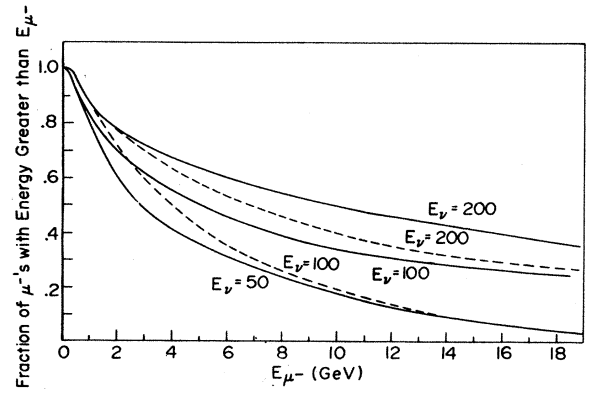

FIG. 5. Plot of the fraction of negative muons with energy greater than a specific energy E_{μ^-}. The solid curves and dashed curves refer to scattering from free protons with $M_W = 5$ GeV/c^2 and 10 GeV/c^2, respectively, and $\kappa = 0$. For example, it is seen that about 70% of the negative muons have an energy greater than 2 GeV when $M_W = 5$ GeV/c^2 and $E_\nu = 100$ GeV.

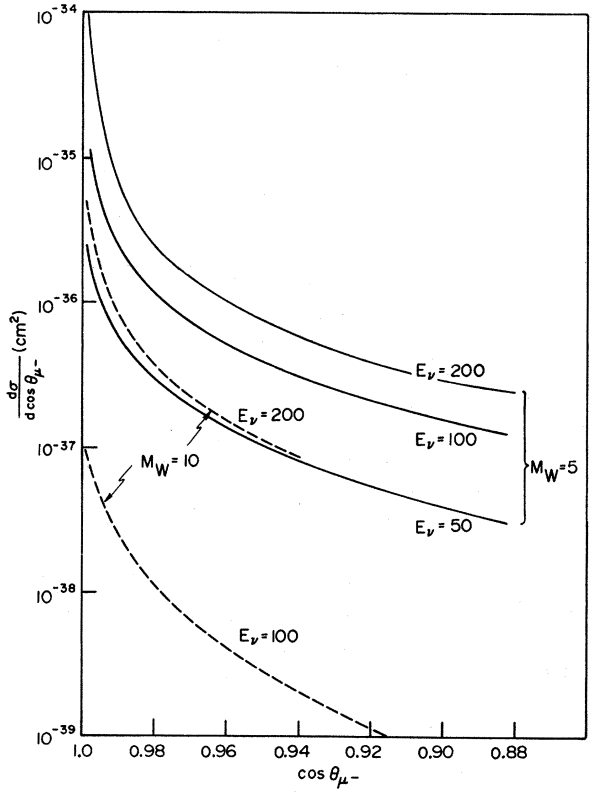

FIG. 7. Plot of $d\sigma/d\cos\theta_{\mu^-}$ in cm^2 for scattering off a free proton. The solid and dashed curves refer to scattering with $M_W = 5$ and 10 GeV/c^2, respectively, and $\kappa = 0$.

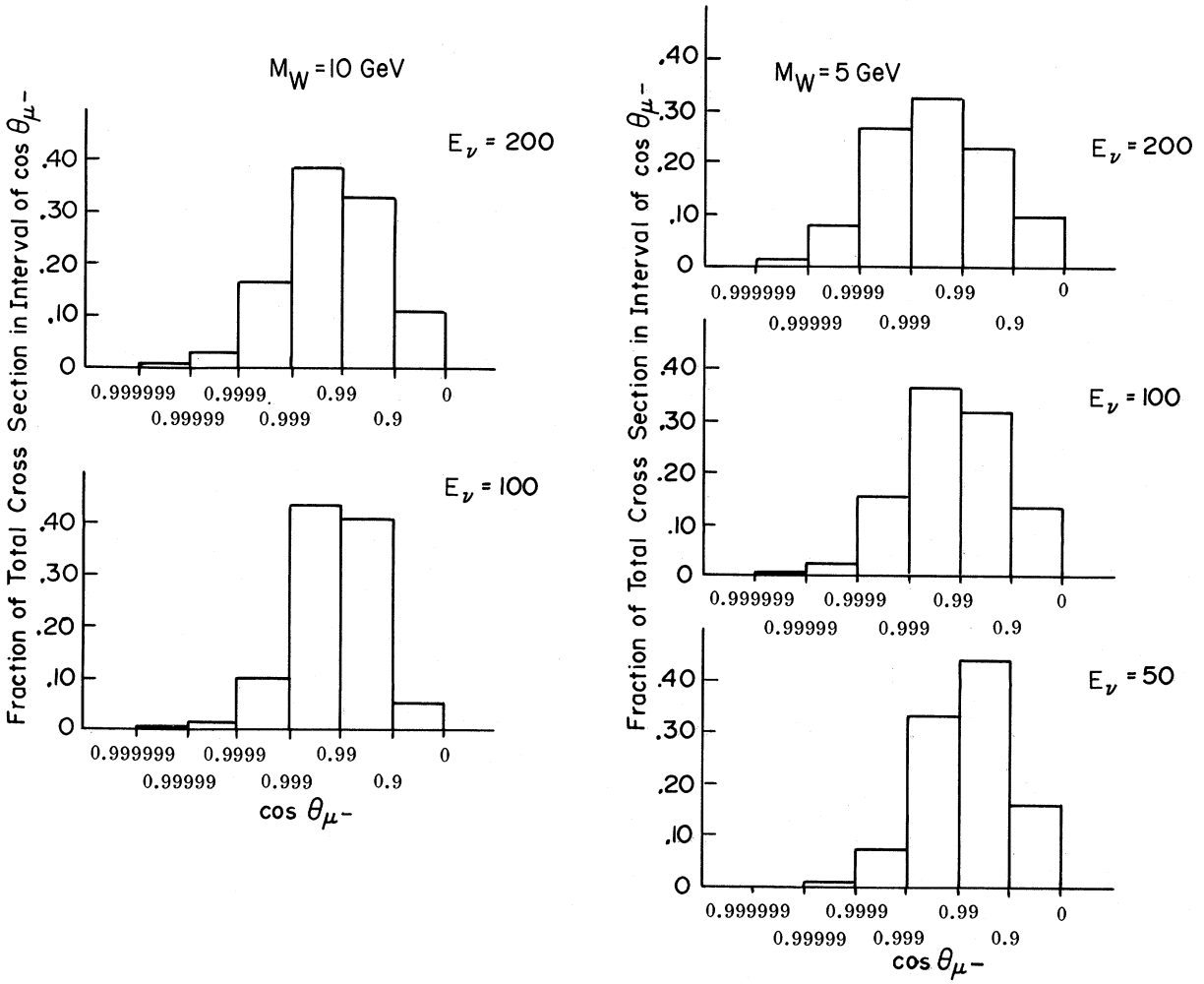

FIG. 8. Histograms of the fraction of the cross section per $\cos\theta_{\mu^-}$ interval for scattering off a free proton. For example, when $E_\nu = 50$ GeV and $M_W = 5$ GeV/c^2, 44% of the total cross section is between $\cos\theta_{\mu^-} = 0.9$ (25.8°) and $\cos\theta_{\mu^-} = 0.99$ (8.1°). We have omitted the small (<2%) histograms for $\cos\theta_{\mu^-} < 0$, and taken $\kappa = 0$.

energies, where the cross section has dropped to an insignificant value. The neutron case resembles that for the proton aside from a diminution due to $G_E(\text{neutron}) \cong 0$.

Turning to the angular distributions given in Fig. 7, we note that they are strongly peaked in the forward direction. Thus, the most effective way of presenting the results appears to be in terms of fraction of cross section per $\cos\theta$ interval. We have done this for all of our cases in Figs. 8 and 9. In all of these histograms, one sees that the μ^- is inside a cone of angle 25° most of the time. In fact, except for the case where $M_W = 5$ and $E_1 = 50$, a much stronger statement can be made: The μ^- is inside of 10° 50% of the time. Very little (less than 20%) of the cross section corresponds to scattering outside of 25°.

The effects of the W anomalous magnetic moment, for all practical purposes, are not striking. Furthermore, the neutron angular distribution resembles the analogous proton distribution. We do get a pronounced shift toward smaller angles in the coherent case as compared with the incoherent single-nucleon scatterings.

IV. THE W-BOSON SPECTRA

The calculation of the energy and angular distributions for the W^+ produced in reaction (1.1) goes in a manner entirely analogous to the prompt muon calculation. For a proton target, we have the following differential cross section in W energy:

$$\frac{d\sigma}{dE_k} = \frac{1}{16\pi^2}\,\frac{\alpha^2 g_W{}^2}{E_1 M_p}\,|\vec{k}| \int_{\cos\theta_{\max}}^{1} d\cos\theta\, \tilde{I}(E_k, \theta). \tag{4.1}$$

Here, $\tilde{I}$ is essentially the function I defined in (3.1) but with the following changes:

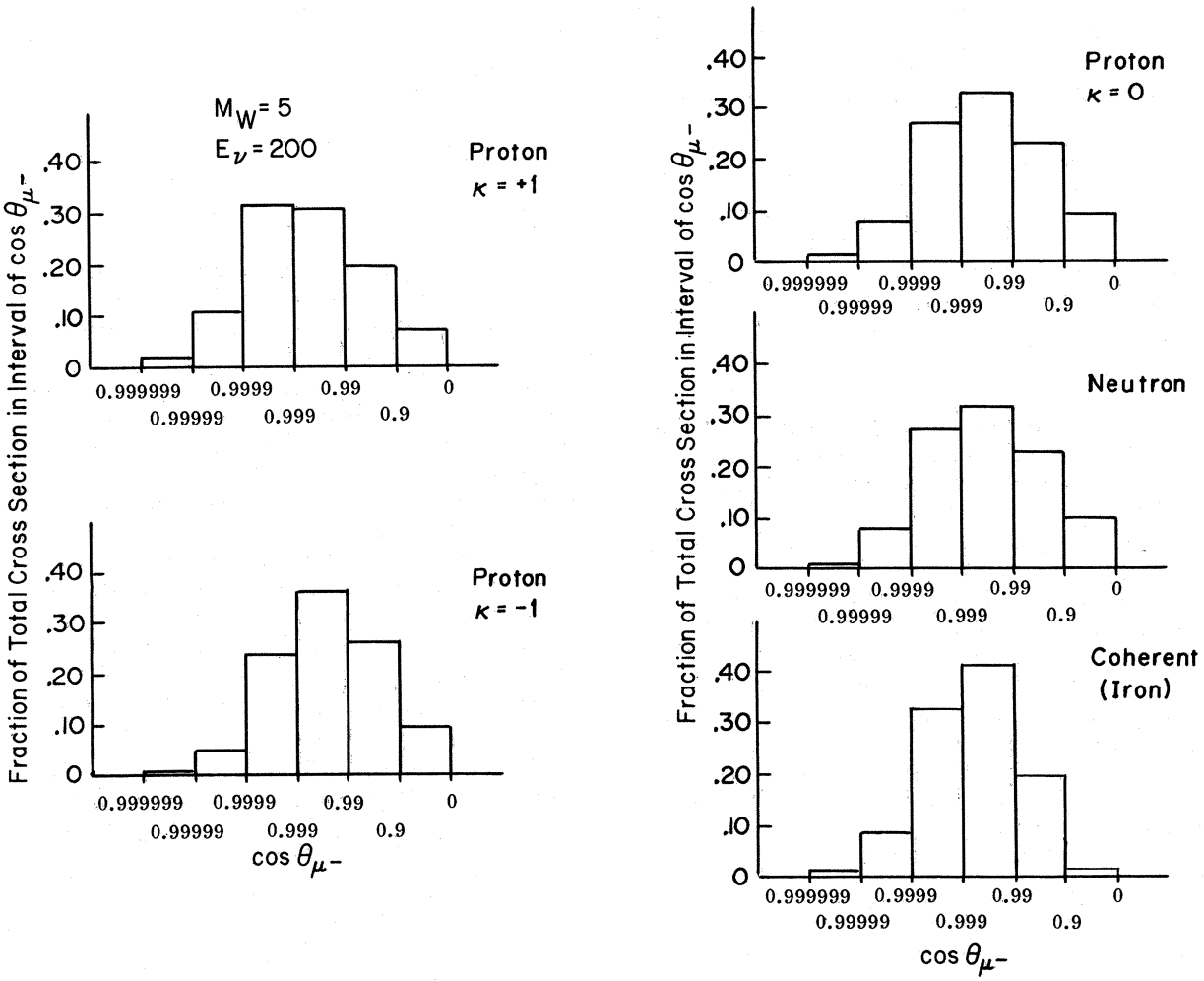

FIG. 9. Histograms of the fraction of the cross section per $\cos\theta_{\mu^-}$ interval for scattering off a free proton, off a free neutron, and off iron. $\kappa = 0$ unless otherwise stated.

$$r \equiv p_2 + k_2 = p_1 + k_1 - k,$$

$$\cos\eta_{\max} = \frac{[4M_p{}^2 r_0{}^2 - (r^2 + M_p{}^2 - \mu^2)^2]^{1/2}}{2M_p|\vec{\mathbf{r}}|} > 0, \tag{4.2}$$

$$E_\pm = \frac{1}{2(r^2 + |\vec{\mathbf{r}}|^2\sin^2\eta)}\{r^0(r^2 + M_p{}^2 - \mu^2) \pm |\vec{\mathbf{r}}|\cos\eta[(r^2 + M_p{}^2 - \mu^2)^2 - 4M_p{}^2(r^2 + |\vec{\mathbf{r}}|^2\sin^2\eta)]^{1/2}\}.$$

The angles here are defined as in Fig. 10.

The lower limit on the $\cos\theta$ integral of (4.1) is now

$$\cos\theta_{\max} = \frac{(\mu + M_p)^2 + 2E_k(E_1 + M_p) - S - 1}{2E_1|\vec{\mathbf{k}}|} > 0. \tag{4.3}$$

Since we consider only the cases where $M_W > M_p$, the W boson cannot be left at rest and must go forward in the laboratory. Thus there is no ambiguity in (4.3) as we had in the μ^- case. For the same reason, the over-all boson energy range in (4.1) is also unambiguously bounded and is given by

$$\left.\begin{matrix} E_{k\max} \\ E_{k\min} \end{matrix}\right\} = \frac{1}{2S}\{(E_1 + M_p)[S + 1 - (\mu + M_p)^2] \pm E_1[(S + 1 - (\mu + M_p)^2)^2 - 4S]^{1/2}\}. \tag{4.4}$$

The W angular differential cross section is

$$\frac{d\sigma}{d\cos\theta} = \frac{1}{16\pi^2}\frac{\alpha^2 g_W{}^2}{E_1 M_p}\int_{E_{k\,\min}(\theta)}^{E_{k\,\max}(\theta)} dE_k |\vec{k}| \tilde{I}(E_k, \theta) \tag{4.5}$$

in the manner of (4.1), where now

$$\left.\begin{matrix} E_{k\,\max}(\theta) \\ E_{k\,\min}(\theta) \end{matrix}\right\} = \frac{1}{2(S+E_1{}^2\sin^2\theta)}\{(E_1+M_p)[S+1-(\mu+M_p)^2] \pm E_1\cos\theta[(S+1-(\mu+M_p)^2)^2 - 4(S+E_1{}^2\sin^2\theta)]^{1/2}\}. \tag{4.6}$$

The over-all θ range corresponds to the forward cone with angle $\theta_{\max}$,

$$\sin^2\theta_{\max} = \frac{[S+1-(\mu+M_p)^2]^2 - 4S}{4E_1{}^2}. \tag{4.7}$$

In the coherent calculation, $M_W < M_p$ (read M_{nucleus} for M_p) and the previous formulas are subject to changes similar to the prompt muon equations in Sec. III. For $S > S_W \equiv S_{\text{thresh}} + (\mu+1)^2/(M_p-1)$, we have $\cos\theta_{\max} = -1$ instead of Eq. (4.3) if that expression < -1. Further, $E_{k\,\min} = 1$ in (4.4), $E_{k\,\min}(\theta) = 1$ in (4.6), and $\theta_{\max} = \pi$ replaces (4.7) for these S values. Since $M_{\text{nucleus}} \gg M_W$ in our coherent case, we are indeed quite far above $S = S_W$.

The procedural remarks stated in Sec. III apply here as well. Plotting $d\sigma/dE_k$ for the array of energies and masses (3.10), we see in Fig. 11 the complementary proton-target curves to those of Fig. 4. Indeed, the W has over 90% of the available energy for these cases in agreement with the minimum $|T|$ argument given earlier. The differences arising by changing κ or the target are seen in Fig. 12; they are visible only below a certain E_k, where the cross section is insignificant.

As far as the boson angular distributions are concerned, it is certainly an understatement to say that the W is peaked in the forward direction. [The peaking is so great that we had to plot $d\sigma/d\cos\theta_W$ against $\log_{10}(1-\cos\theta_W)$.] This is qualitatively seen in Fig. 13 and quantitatively described by histograms in Figs. 14 and 15. In general, virtually all of the total cross section for the cases under consideration corresponds to the W lying inside a cone of one or two degrees. This is expected, of course, in view of the energy distributions, since if the W has all of the energy it necessarily has to go straight ahead in the laboratory. The $\kappa = \pm 1$ proton calculations and the neutron ($\kappa = 0$) calculation are similar to the proton ($\kappa = 0$) results and the coherent case is understandably peaked more forward.

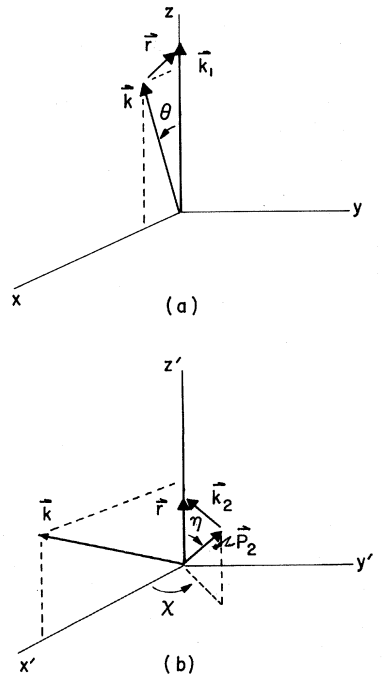

FIG. 10. Coordinate system used in the calculation of W^+ spectra.

V. THE W-BOSON POLARIZATION

We address ourselves now to the calculation of the average density matrix defined by

$$\bar{\rho}_{ab}(E_1) = \frac{1}{\sigma_{\text{tot}}(E_1)}\frac{1}{32\pi^3}\frac{\alpha^2 g_W{}^2}{E_1 M_p}\int \frac{d^3k_2}{E_2}\frac{d^3k}{E_k}\frac{d^3p_2}{E_{p_2}} \times \delta^4(k_1 - q - k_2 - k) T^{-2} P_{\nu\mu}\epsilon^*_\alpha(a)\epsilon_\beta(b) L^{\beta\nu\mu\alpha} \tag{5.1}$$

using the notation of Eq. (2.3). It is to be understood here that we are calculating the $\vec{k}$-averaged density matrix $\bar{\rho}$ (which is sufficiently informative

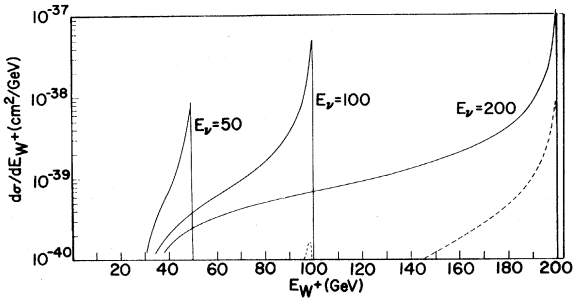

FIG. 11. Plot of $d\sigma/dE_{W^+}$ in cm^2/GeV for scattering off a free proton. The solid lines are for $M_W = 5$ GeV/c^2, the dashed lines are for $M_W = 10$ GeV/c^2, and $\kappa = 0$.

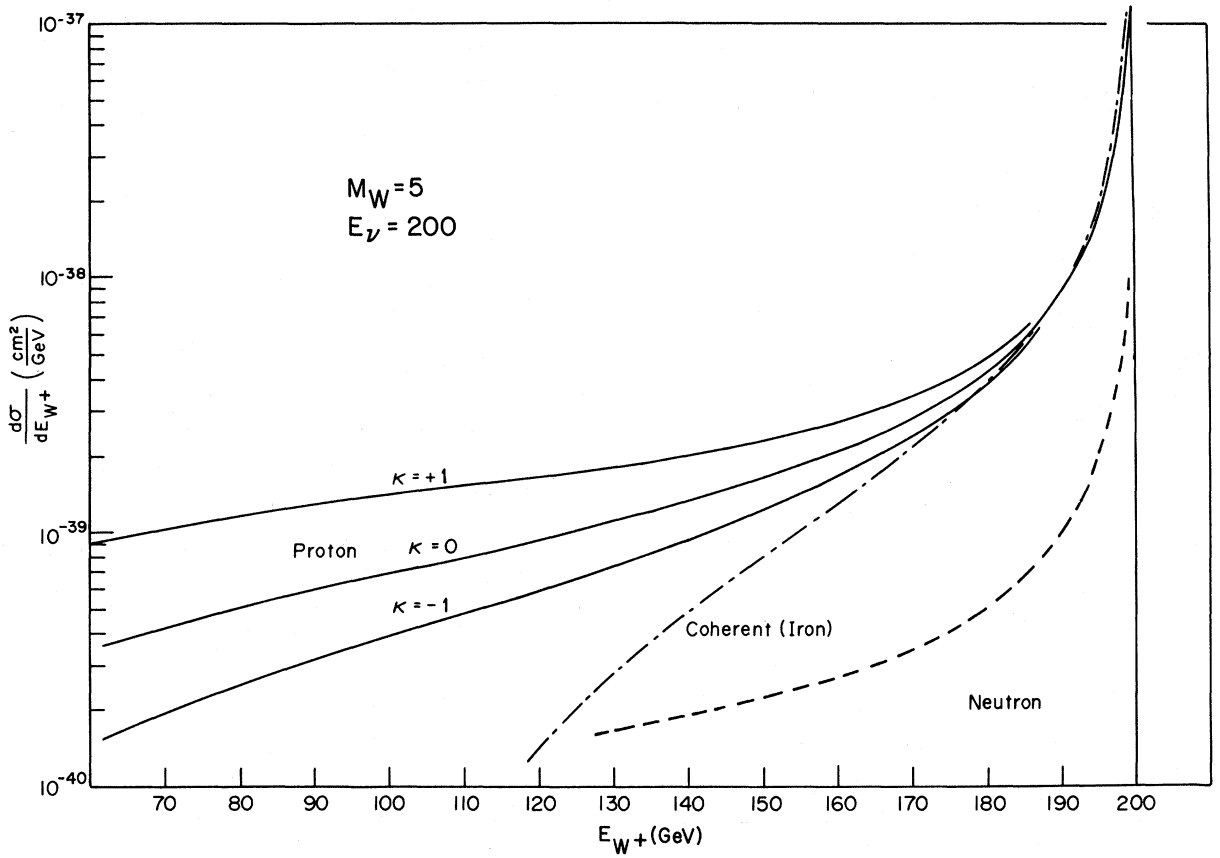

FIG. 12. Plot of $d\sigma/dE_{W^+}$ in cm^2/GeV for scattering off a free proton, a free neutron, and an iron nucleus target (normalized per proton). All curves are drawn for $E_\nu = 200$ GeV and $M_W = 5$ GeV/c^2. $\kappa = 0$ unless otherwise stated.

since the W has been shown to be within a degree or so of the forward direction in all cases). An appropriate linear orthogonal basis is

$$\epsilon^\alpha(1) = \left(0, \frac{\vec{k}_1 \times \vec{k}}{|\vec{k}_1 \times \vec{k}|}\right) = (0, \hat{y}),$$

$$\epsilon^\alpha(2) = \left(0, \frac{\vec{k} \times (\vec{k}_1 \times \vec{k})}{|\vec{k} \times (\vec{k}_1 \times \vec{k})|}\right) = (0, -\cos\theta\,\hat{x} + \sin\theta\,\hat{z}), \quad (5.2)$$

$$\epsilon^\alpha(3) = (|\vec{k}|, E_k \hat{k}) = (|\vec{k}|, E_k \sin\theta\,\hat{x} + E_k \cos\theta\,\hat{z}),$$

according to the angles defined in Fig. 10(a). It is seen that this basis changes when k does; also, it satisfies the subsidiary condition $k \cdot \epsilon(a) = 0$ for all a. The normalization is such that $\epsilon^2(a) = -1$ so we indeed satisfy $\sum_a \epsilon^*_\alpha(a)\epsilon_\beta(a) = -g_{\alpha\beta} + k_\alpha k_\beta = K_{\alpha\beta}$.

Since we have included the *unpolarized* total cross section in the denominator of our definition (5.1), it follows that $\mathrm{Tr}\bar{\rho} = 1$. This serves as a check on the diagonal terms if σ_{tot} is taken from the calculations done in I. The lepton trace implied by $L^{\beta\nu\mu\alpha}$ has been calculated using Veltman's CDC 6600 algebraic computer program and the result[16] is in terms of pseudoscalar [e.g., $\epsilon_{\mu\nu\rho\tau}\epsilon^{*\mu}(a)\epsilon^\nu(b) \times k_1^\rho k^\tau$, etc.] as well as scalar dot products. We have evaluated these by working out the relations between the angles defined in Fig. 10.

We also know that $\bar{\rho}_{ab} = \bar{\rho}^*_{ba}$. Then by time reversal invariance,[8] the elements $\bar{\rho}_{12} = -\bar{\rho}_{21}$ and $\bar{\rho}_{13} = -\bar{\rho}_{31}$ are purely imaginary and $\bar{\rho}_{23} = \bar{\rho}_{32}$ is real. This gives us a check on the off-diagonal elements. We also repeated the coherent calculation performed by Bell and Veltman[8] for a copper target (with a Fermi form factor) at $M_W = M_p$, $E_1 = 6$, and $\kappa = 0$. Our results were in excellent agreement for the six independent elements (within 1% for five elements and 10% for $\bar{\rho}_{13}$).

The strong left-circular polarization present for the region considered by Bell and Veltman persists at the higher energies and masses treated here. Our results for the six density-matrix elements are given in Table II for the cases discussed in Sec. III. There we see the approximate equality $\rho_{11} \approx \rho_{22} \approx -i\rho_{12}$ together with the fact that the other elements are much smaller than these. Hence the density matrix is close to being diagonalized in the orthogonal circular basis[17]

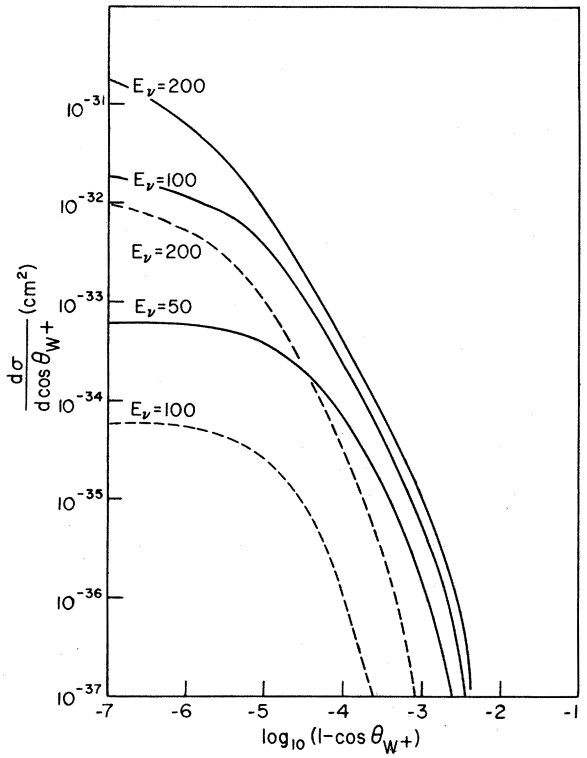

FIG. 13. Plot of $d\sigma/d\cos\theta_{W^+}$ in cm^2 versus $\log_{10}(1-\cos\theta_{W^+})$ for scattering off a free proton. The solid curves refer to $M_W=5$ GeV/c^2, the dashed curves to $M_W=10$ GeV/c^2, and $\kappa=0$.

$$\epsilon^\alpha(+)=(0,-(\tfrac{1}{2})^{1/2}[\vec{\epsilon}(1)+i\vec{\epsilon}(2)]),\ \text{right-circular};$$
$$\epsilon^\alpha(-)=(0,(\tfrac{1}{2})^{1/2}[\vec{\epsilon}(1)-i\vec{\epsilon}(2)]),\ \text{left-circular};\quad (5.3)$$
$$\epsilon^\alpha(0)=\epsilon^\alpha(3),\ \text{longitudinal}.$$

The plot of the diagonal element $\bar{\rho}_{--}$ in the circular basis as a function of E_1 is shown in Fig. 16 for proton targets and $\kappa=0,\pm1$. This shows that the W^+ maintains a high degree of left handedness even for extremely high energies at $M_W=5$, although we do see a slow decrease in polarization with increasing neutrino energy.

We find also that the W^+ loses its left-handed spin character for energies E_k well below the maximum value of E_k allowed or, putting it another way, for angles close to the maximum opening angle permitted. (This was seen in our detailed study of ρ as a function of θ and E_k.) However, these regions do not contribute anything to the cross section and, indeed, this is consistent with the results shown in Table II and Fig. 16.

The reason for the sharp left-handed polarization is tied to the crucial role of the muon propagator. After the cancellation dictated by gauge invariance (described in I) the muon propagator diagram in Fig. 1 dominates and controls the helicity of the W. The reader is referred to Bell and Veltman[8] for a more detailed discussion. The lack of sharp polarization seen by Reiff[4] in reaction (1.2) is related to the absence of this muon propagator enhancement in that reaction. We thank J. Reiff for a communication regarding this point.

VI. THE DECAY-MUON ANGULAR DISTRIBUTION

We have just seen that the W^+ is almost completely in a negative-helicity state in the laboratory. Transforming back to the W's rest frame, this implies that the μ^+ in the decay (1.3) should have an angular distribution in this frame resembling $(1-\cos\theta^*)^2$, where θ^* is the angle of the μ^+ with respect to the original direction of the W^+ in the laboratory.[8,9] Therefore, we already have a good idea of what the laboratory μ^+ angular distribution is going to be since the W emerges essentially collinear with the incoming neutrino beam.

In this section, we check the above notion by actually calculating the μ^+ angular distribution in the laboratory. To do this, we utilize the differential decay matrix for (1.3),

TABLE II. The density-matrix elements defined in Eq. (5.1) calculated according to the basis given in Eq. (5.2) for various energies, masses, targets, and κ values.

Target	M_W (GeV/c^2)	E_ν (GeV)	κ	ρ_{11}	ρ_{22}	ρ_{33}	ρ_{12}	ρ_{13}	ρ_{23}
Proton	5	50	0	0.494	0.460	0.046	+0.474i	−0.067i	−0.068
	5	100	0	0.494	0.447	0.059	+0.463i	−0.063i	−0.059
	5	200	+1	0.498	0.400	0.103	+0.408i	−0.029i	−0.055
	5	200	0	0.491	0.441	0.068	+0.452i	−0.059i	−0.050
	5	200	−1	0.466	0.487	0.047	+0.460i	−0.082i	−0.064
	10	100	0	0.498	0.486	0.016	+0.492i	−0.047i	−0.049
	10	200	0	0.498	0.470	0.032	+0.481i	−0.055i	−0.056
Neutron	5	200	0	0.484	0.417	0.099	+0.424i	−0.062i	−0.041
Iron	5	200	0	0.499	0.477	0.024	+0.485i	−0.047i	−0.049

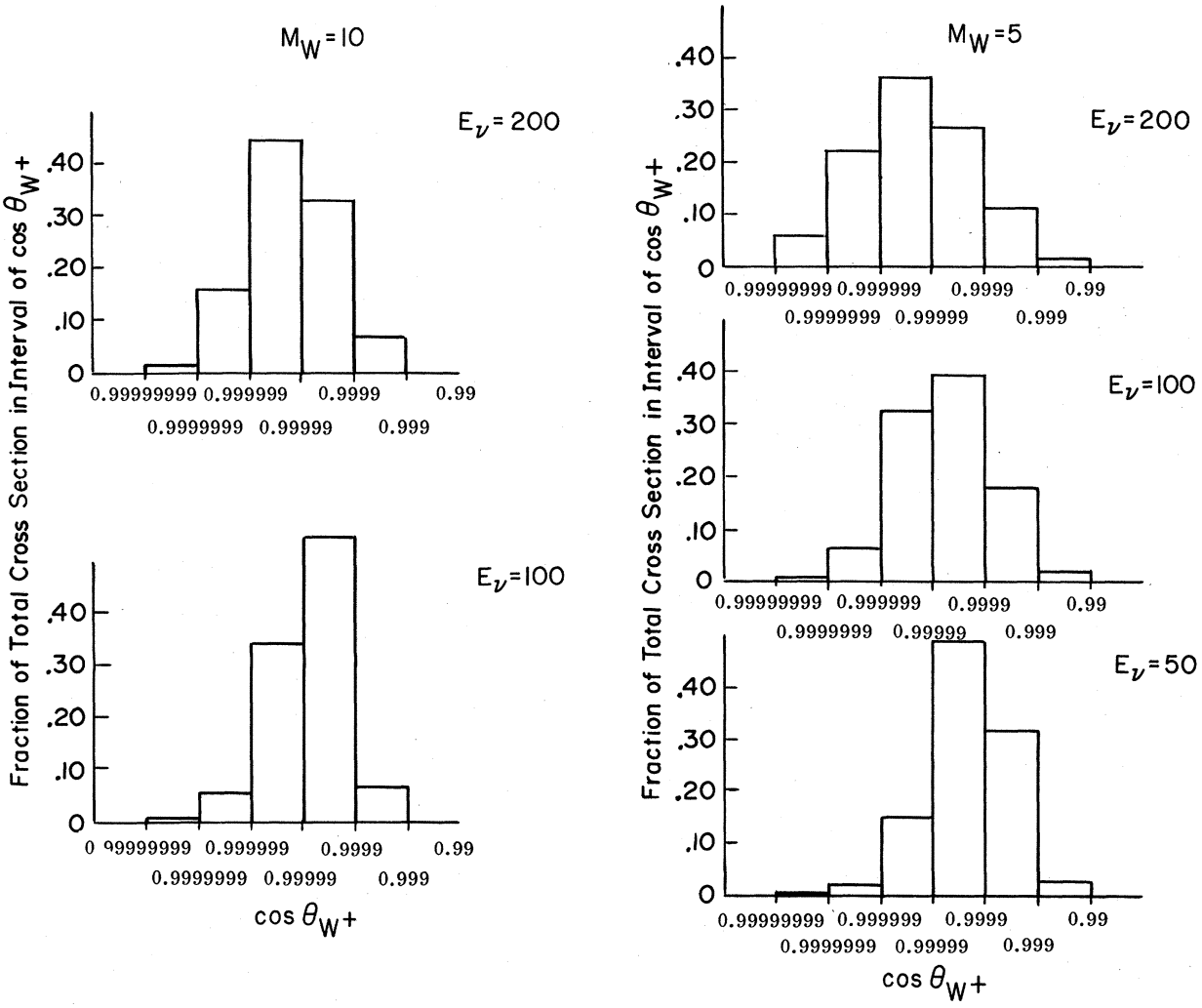

FIG. 14. Histograms of the fraction of cross section per $\cos\theta_{W^+}$ interval for scattering off of a free proton with $\kappa = 0$. For example, when $E_\nu = 50$ GeV and $M_W = 5$ GeV/c^2, 48% of the total cross section is between $\cos\theta_{W^+} = 0.9999$ (0.8°) and $\cos\theta_{W^+} = 0.999\,99$ (0.3°).

$$dR_{ba} = \frac{1}{E_k}\frac{g_W^2}{2\pi^2}\epsilon_\beta^*(b)\epsilon_\alpha(a)d\Omega' E_2'^2(k_2'^\beta k_1'^\alpha + k_1'^\beta k_2'^\alpha - k_1'\cdot k_2' g^{\beta\alpha} + i\epsilon^{\beta\mu\alpha\nu}k_{1\mu}' k_{2\nu}') + O(\mu^2), \tag{6.1}$$

where k_1' and k_2' (satisfying $k_1' + k_2' = k$) are the four-momenta of the decay neutrino and decay muon, respectively. Also, E_2' is the laboratory energy of the μ^+ given by

$$E_2' = \frac{1}{2(E_k - |\vec{k}|\cos\gamma)} + O(\mu^2) \tag{6.2}$$

if the angle between $\vec{k}$ and $\vec{k}_2'$ is γ in the laboratory. The solid angle $\Omega' = \Omega'(\theta', \phi')$ refers to the decay μ^+ in the system of Fig. 10(a).

We are now led to calculate the angular distribution of the μ^+ according to (neglecting muon mass terms)

$$\frac{dN}{d\Omega'} = \frac{1}{\sigma_{\text{tot}}}\frac{1}{32\pi^3}\frac{\alpha^2 g_W^2}{E_1 M_p}\int\frac{d^3k_2}{E_2}\frac{d^3k}{E_k}\frac{d^3p_2}{E_{p_2}}\delta^4(k_1 - q - k_2 - k)$$

$$\times\frac{3}{\pi}E_2'^2 T^{-2}P^{\nu\mu}L_{\beta\nu\mu\alpha}(k_2'^\beta k_1'^\alpha + k_1'^\beta k_2'^\alpha - \tfrac{1}{2}g^{\beta\alpha} + i\epsilon^{\beta\mu\alpha\nu}k_{1\mu}' k_{2\nu}'). \tag{6.3}$$

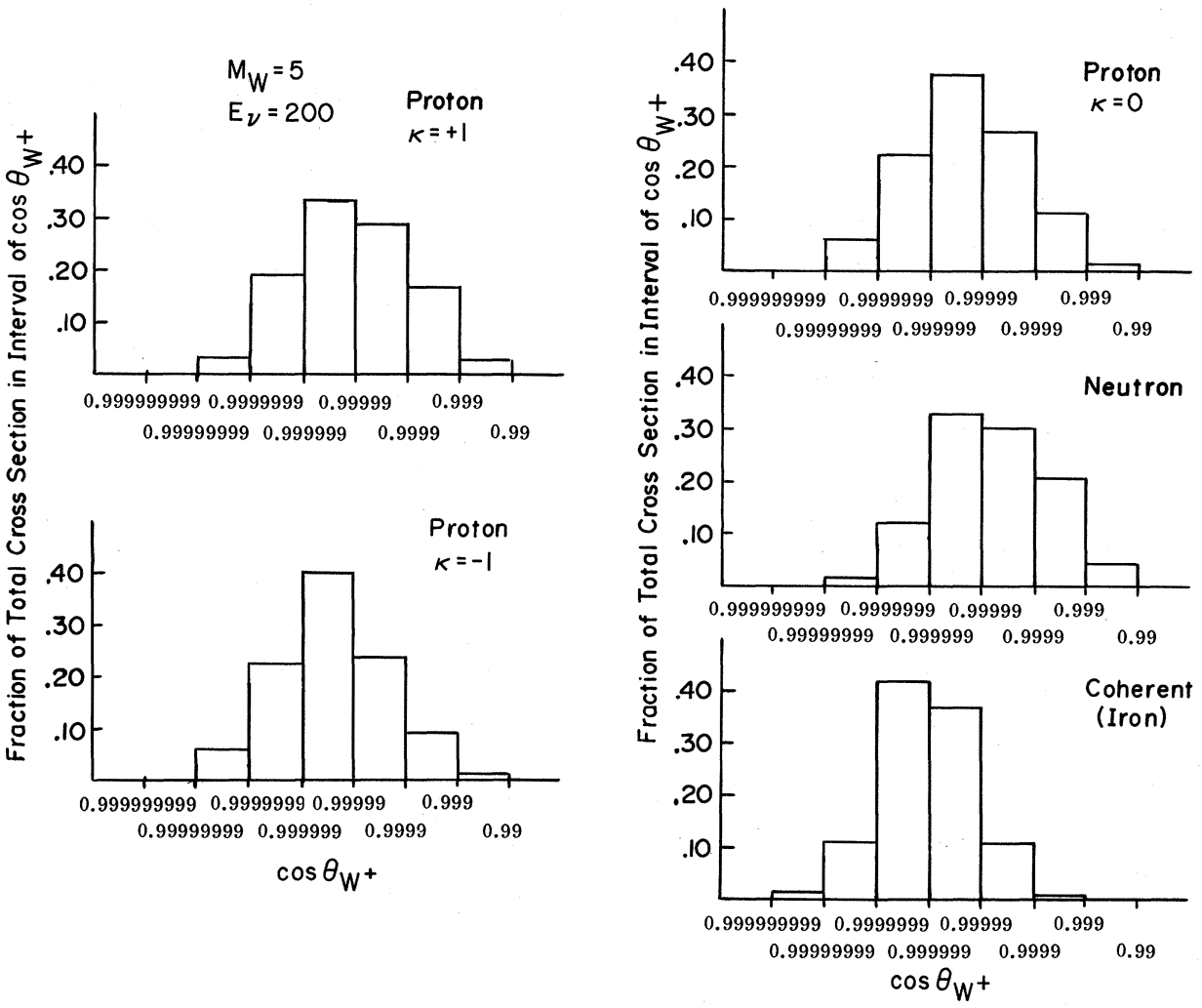

FIG. 15. Histograms of the fraction of cross section per $\cos\theta_{W^+}$ interval for free proton targets, free neutron targets, and an iron nucleus target. All curves correspond to $E_\nu = 200$ GeV and $M_W = 5$ GeV/c^2. $\kappa = 0$ unless otherwise stated.

This is the average distribution of the decay muon (gotten by dividing through by the total rate R for a given k) for a given neutrino energy and target; consistent with the neglect of the muon mass terms, the limits on the integrals are the same as in Sec. IV. In clarification of this last remark, we note that there is no additional constraint on the W even if θ' and ϕ' of a massless muon are fixed. There is now some dependence in (6.3) on the azimuthal angle of the W which is to be integrated out.

The trace-tensor product of Eq. (6.3) has been evaluated using Veltman's algebraic computer program, and we do six integrations numerically in the calculations of this section [the six are needed in order to check that N calculated from (6.3) is unity]. The results for $\sigma_{\text{tot}}\, dN/d\cos\theta_{\mu^+}$, covering the set of energies and masses in (3.10) are plotted in Fig. 17 ($\kappa = 0$ here and the target is the proton). Additionally, we have superimposed the laboratory distribution [see (6.4)] corresponding to the muon distribution $(1 - \cos\theta^*)^2$ for a left-handed W with energy $E_k = E_1$ and $\theta = 0$ on these curves. It is gratifying that the results of Sec. V (the W takes all of the energy, goes straight ahead, and is left-circularly polarized) thus agree with this independent calculation of the μ^+ angular spectrum. Another presentation of the angular distribution results is seen in the histograms of Fig. 18. These results are similar to the μ^- ones in Fig. 8; however, the energy distributions discussed below are quite different.

By writing a bin selection step into the previous numerical integration, we were able also to calculate the μ^+ energy distributions which are illustrated in Fig. 19. These show that the decay μ^+ has a much larger average energy than the prompt μ^-

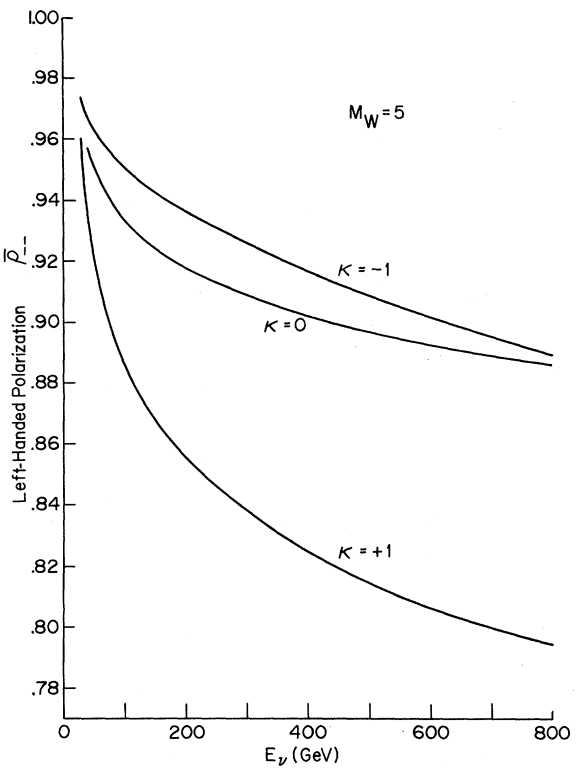

FIG. 16. Plot of the average left-handed polarization $\bar{\rho}_{--}$ as a function of the incident neutrino energy for a free proton and $\kappa = +1$, 0, and -1.

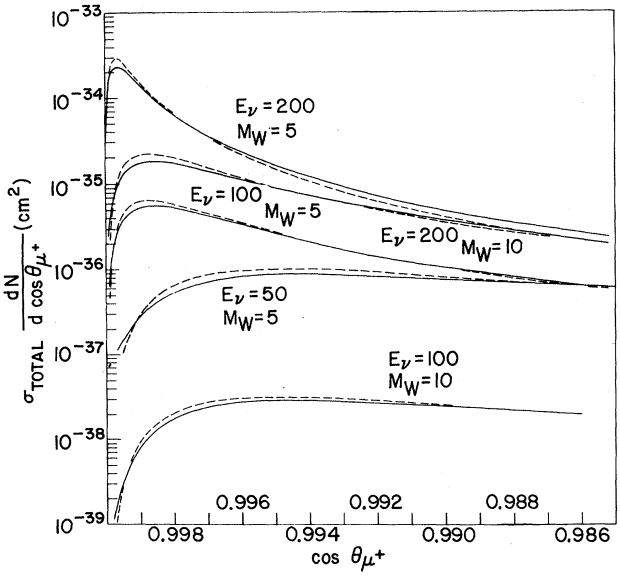

FIG. 17. Plot of $\sigma_{tot} dN/d\cos\theta_{\mu^+}$ in cm^2 for a proton target with $\kappa = 0$. The solid lines are results of our full calculation whereas the dashed lines are obtained by transforming the $(1 - \cos\theta^*)^2$ c.m. distribution, normalized to the same total cross section.

as one would expect from the W results. In addition, these μ^+ curves agree well with the simple energy distribution [see (6.5)] derived from the $(1 - \cos\theta^*)^2$ formula and (6.2).

Thus the simple Lorentz transformation of $(1 - \cos\theta^*)^2$ (see Fig. 20 for example) can be used as an accurate guide since the W momentum and polarization are so sharp. Explicitly, we have for the transformed angular distribution,

$$\frac{dN}{d\cos\theta_{\mu^+}} = \frac{3}{8} \frac{1}{\gamma_W^2(1 - \beta_W\cos\theta_{\mu^+})^2} \left(1 + \frac{\beta_W - \cos\theta_{\mu^+}}{1 - \beta_W\cos\theta_{\mu^+}}\right)^2, \tag{6.4}$$

and for the energy distribution,

$$\frac{dN}{dE_{\mu^+}} = \frac{3}{4} \frac{1}{M_W} \frac{1}{\beta_W\gamma_W} \left[1 + \frac{1}{\beta_W}\left(1 - \frac{2E_{\mu^+}}{\gamma_W M_W}\right)\right]^2, \tag{6.5}$$

where $\gamma_W = E_k/M_W$ and $\beta_W = |\vec{k}|/E_k$. These distributions are normalized to $N = 1$ and the muon mass has been neglected.

From the above remarks, the angular and energy distributions in other simple decay modes (e.g., $\pi^+\pi^0$ and $e^+\nu_e$) can be predicted. Of course, the e^+ in the $e^+\nu_e$ decay follows the μ^+ distributions discussed above since the μ^+ mass has been neglected. For the $\pi^+\pi^0$ decay, the left-handed W implies a $\sin^2\theta^*$ distribution for either pion.[8,9]

VII. DEEP-INELASTIC EFFECTS

Particular hadronic resonances formed at the photon-proton vertex are not expected to be of consequence here since it has been seen[4,14] that their contributions to the total cross section for W production are substantially reduced compared to the "elastic" photon interaction. The fact that the "deep"-inelastic channels taken together give a comparable (same order of magnitude) total cross section[18] motivates us to calculate explicitly the effects of the inclusion of these channels in a manner analogous to that of I.

We thus wish to sum over the undetected final hadron states produced at the nucleon-photon-hadron vertex (see Fig. 21) where now $p_2^2 = W^2$ and the deep-inelastic form factors are taken from a fit to the SLAC data.[19] For example, the prompt muon spectra from these channels is calculated according to

$$d^2\sigma_\mu = \frac{1}{16\pi^2} \frac{\alpha^2 g_W^2}{E_1 M_p} |\vec{k}_2| \, dE_2 d\cos\theta \times \int_{W^2\,min}^{W^2\,max} dW^2 I_{inel}(E_2, \theta, W), \tag{7.1}$$

where I_{inel} is defined in a way parallel to I of Eq. (3.1) but with the following changes:

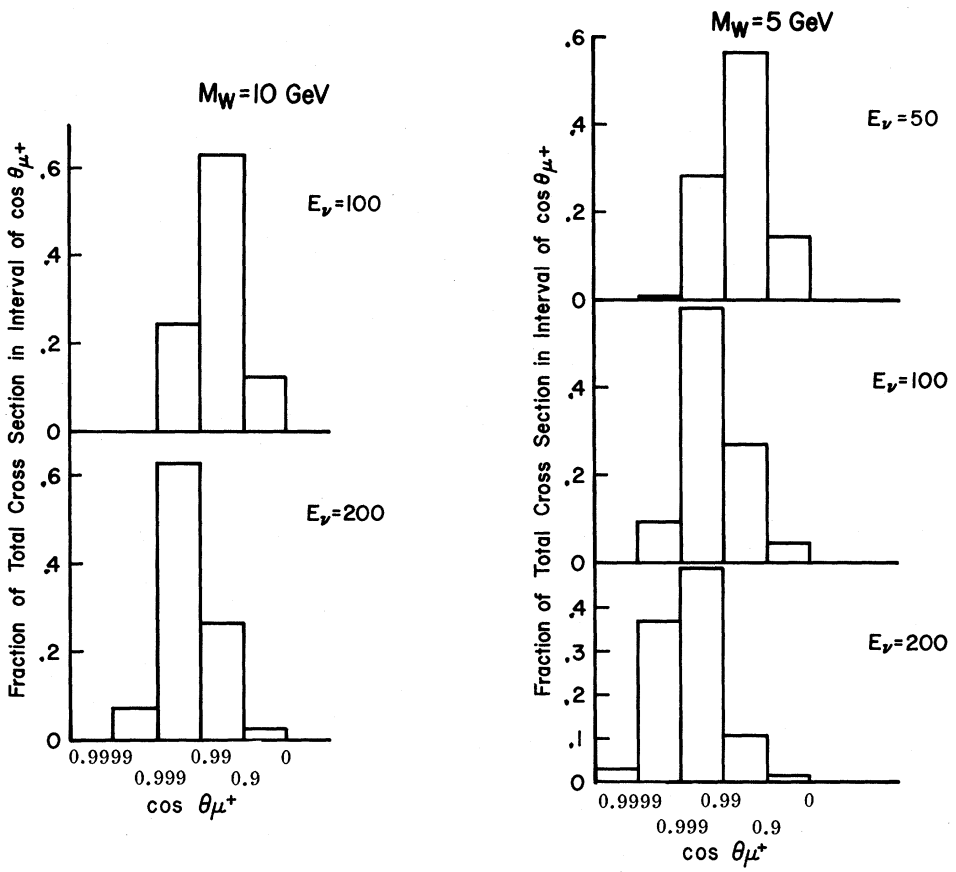

FIG. 18. Histograms of the fraction of cross section per $\cos\theta_{\mu^+}$ interval for scattering off a free proton and $\kappa=0$. For example, when $E_\nu=50$ GeV and $M_W=5$ GeV/c^2, 56% of the total cross section is between $\cos\theta_{\mu^+}=0.9$ (25.8°) and $\cos\theta_{\mu^+}=0.99$ (8.1°). We have omitted the small histograms for $\cos\theta_{\mu^+}<0$.

$$\cos\eta_{\max}=\frac{[4W^2r_0{}^2-(r^2+W^2-1)^2]^{1/2}}{2W|\vec{r}|}>0,$$

$$P_{\nu\mu}\to P_{\nu\mu}^{\text{inel}}=2M_p\left[-\left(g_{\nu\mu}-\frac{q_\nu q_\mu}{T}\right)W_1(T,\nu)+\frac{1}{M_p{}^2}\left(p_{1\nu}-\frac{p_1\cdot q}{T}q_\nu\right)\left(p_{1\mu}-\frac{p_1\cdot q}{T}q_\mu\right)W_2(T,\nu)\right], \tag{7.2}$$

$$\nu\equiv q^0=\frac{p_1\cdot q}{M_p}=\frac{1}{2M_p}(W^2-M_p{}^2-T).$$

Furthermore, the roots $E_\pm$ are changed from (3.2) by the replacement $M_p{}^2\to W^2$.

The limits on W in Eq. (7.1) read

$$W_{\max}=[S+\mu^2-2E_2(E_1+M_p)+2|\vec{k}_2|E_1\cos\theta]^{1/2}-1,$$
$$W_{\min}=M_p+m_{\text{pion}}. \tag{7.3}$$

The expressions for $\theta_{\max}$ in (3.2) and (3.9), and for the limits in (3.5) and (3.8) are changed according to the replacement $M_W\to M_W+W_{\min}-M_p$. (Note that M_W has been set equal to unity in these formulas.) Here, as in I, we use the assumption of scaling for νW_2, we neglect the longitudinal photoabsorption cross section,[20] and we employ a crude fit to the data.[19] That is,

$$W_1=\left(\frac{\nu^2-T}{-T}\right)\frac{W_2}{1+R},\quad R\equiv\frac{\sigma_l}{\sigma_\tau}\cong 0;$$
$$\nu W_2=F(\omega),\quad \omega\equiv -2M_p\nu/T; \tag{7.4}$$
$$F(\omega)\cong 0.4(1-e^{-(\omega-1)})/(1+\tfrac{1}{20}\omega).$$

There are two remarks in order here. First, the choice for W_1, with $R=0$ scales for $\nu\gg M_p$. Second, we probably overestimate the small-W region since the inelastic channels are extended all

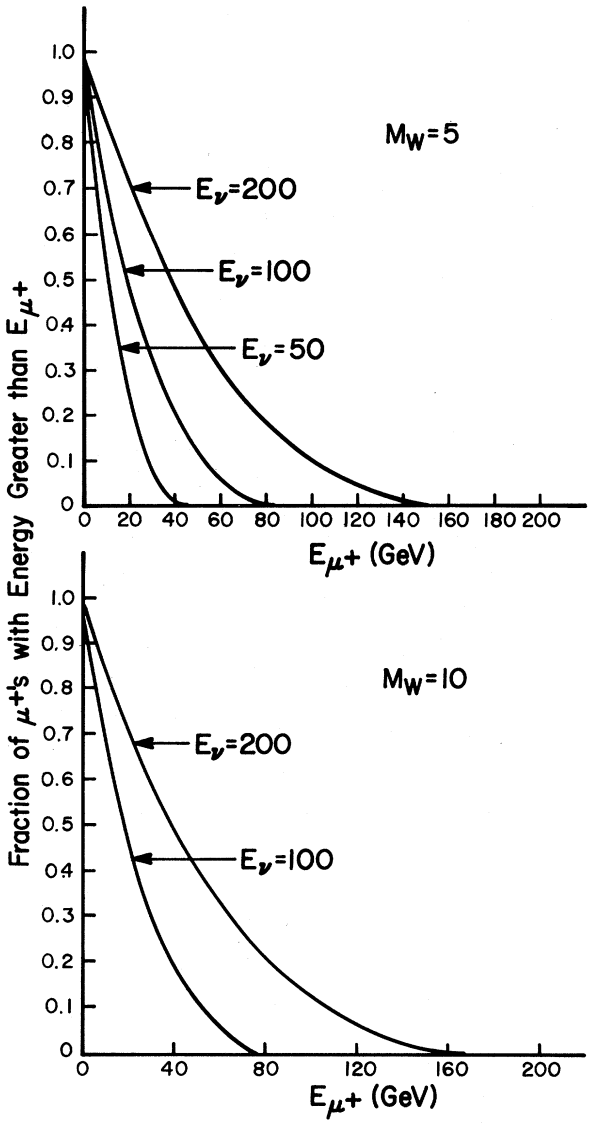

FIG. 19. Plot of the fraction of positive muons with energy greater than a specific energy E_{μ^+}. The target is the free proton, we take $\kappa=0$, $M_W=5$ and 10 GeV/c^2. For example, it is seen that 20% of the positive muons have an energy greater than 40 GeV when $M_W=5$ GeV/c^2 and $E_\nu=100$ GeV.

the way down to $W=M_p+m_{\text{pion}}$. This error is partially compensated for by the omission of the $N^*(1236)$ contribution.

The W-boson spectra for this contribution is found to be

$$d^2\sigma_W=\frac{1}{16\pi^2}\frac{\alpha^2 g_W{}^2}{E_1 M_p}|\vec{k}|\,dE_k\,d\cos\theta \times\int_{W^2\min}^{W^2\max} dW^2\tilde{I}_{\text{inel}}(E_k,\theta,W^2), \tag{7.5}$$

where $\tilde{I}_{\text{inel}}$ is changed from $\tilde{I}$ of (4.1) via

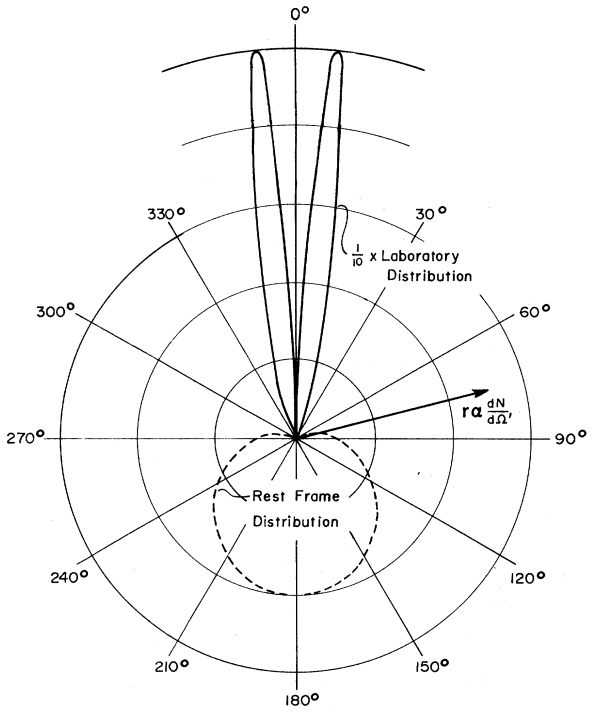

FIG. 20. Plot of the μ^+ angular distribution (arbitrary units) in the W^+ rest frame (dashed curve) and the laboratory frame (solid curve) according to the $(1-\cos\theta^*)^2$ distribution for $\gamma_W=E_k/M_W=10$.

$$\cos\eta_{\max}=\frac{[4W^2r_0{}^2-(r^2+W^2-\mu^2)^2]^{1/2}}{2W|\vec{r}|}>0, \tag{7.6}$$

$$P_{\nu\mu}\to P_{\nu\mu}^{\text{inel}}.$$

Also, the $E_\pm$ of (4.2) can be used here if we replace $M_p{}^2$ by W^2. The limits on W in (7.5) are given by

$$W_{\max}=[S+1-2E_k(E_1+M_p)+2|\vec{k}|E_1\cos\theta]^{1/2}-\mu, \tag{7.7}$$

$$W_{\min}=M_p+m_{\text{pion}}.$$

The $\theta_{\max}$ equations in (4.3) and (7.7), the $E_{k\max}$ and

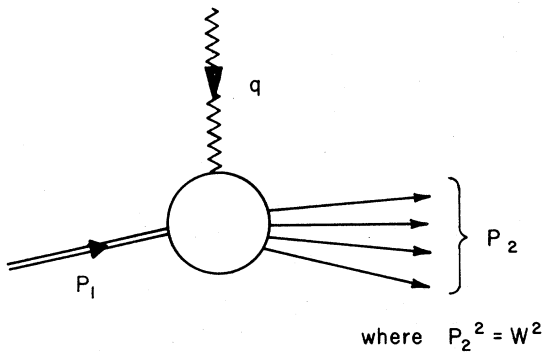

FIG. 21. The general inelastic hadron vertex.

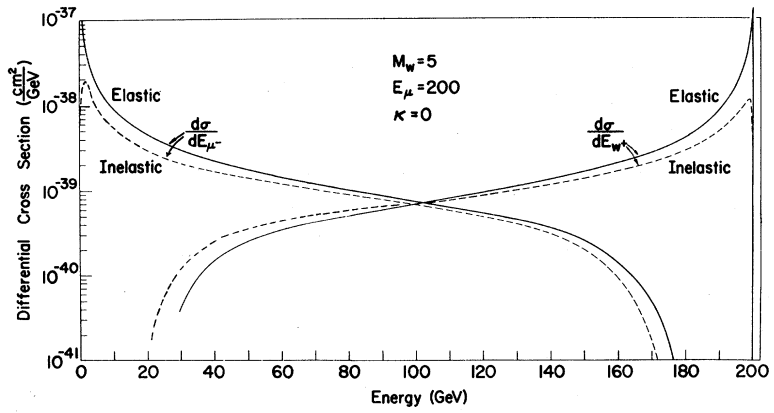

FIG. 22. Comparison plot of $d\sigma/dE_{\mu^-}$ and $d\sigma/dE_{W^+}$ for scattering via the elastic proton vertex (solid lines) and the inelastic proton vertex (dashed lines).

$E_{k\,\min}$ formulas in (4.4) and (4.6), and the remarks in the paragraph after Eq. (4.7), should be modified by the recipe $\mu \to \mu + W_{\min} - M_p$.

With these details out of the way, we are now ready to discuss the spectra for deep-inelastic channels. As a remark in passing, the evaluation of the trace product needed here was again easily handled by the algebraic computer program. (The substitution routines in Veltman's program are extremely useful in all of these calculations.) Our results here are very similar to the "elastic" proton calculations. As an illustration at $M_W = 5$, $E_1 = 200$, and $\kappa = 0$, $d\sigma/dE_2$ and $d\sigma/dE_k$ as seen in Fig. 22 and $d\sigma/d\cos\theta_{\mu^-}$ and $d\sigma/d\cos\theta_{W^+}$ as seen in Fig. 23 resemble their counterpart proton results. (The total cross section is less by a factor of $\frac{3}{5}$.) This has been found to be generally the case.

The resemblance of the calculations (proton and deep inelastic) is simply due to the damping of the large-W channels. In Fig. 24, we show $d\sigma/dW$

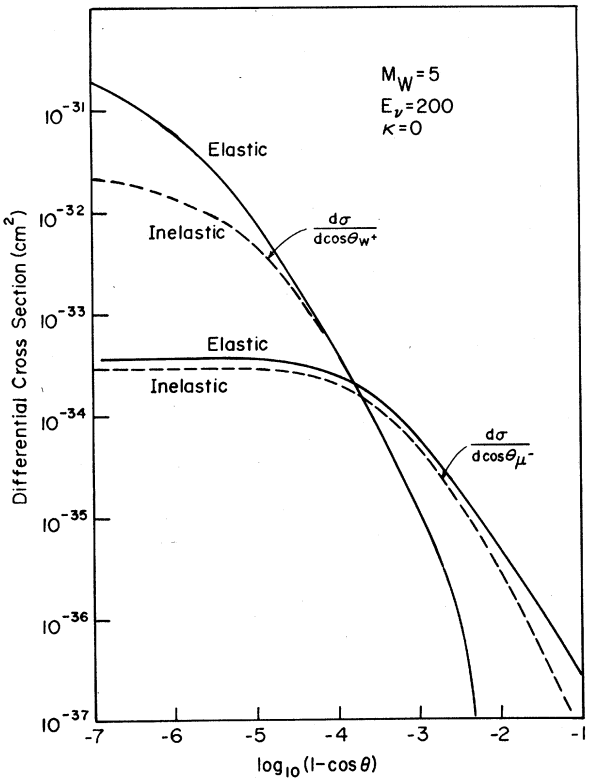

FIG. 23. Comparison plot of $d\sigma/d\cos\theta_{\mu^-}$ and $d\sigma/d\cos\theta_{W^+}$ for scattering via the elastic proton vertex (solid lines) and the inelastic proton vertex (dashed lines) versus $\log_{10}(1-\cos\theta)$.

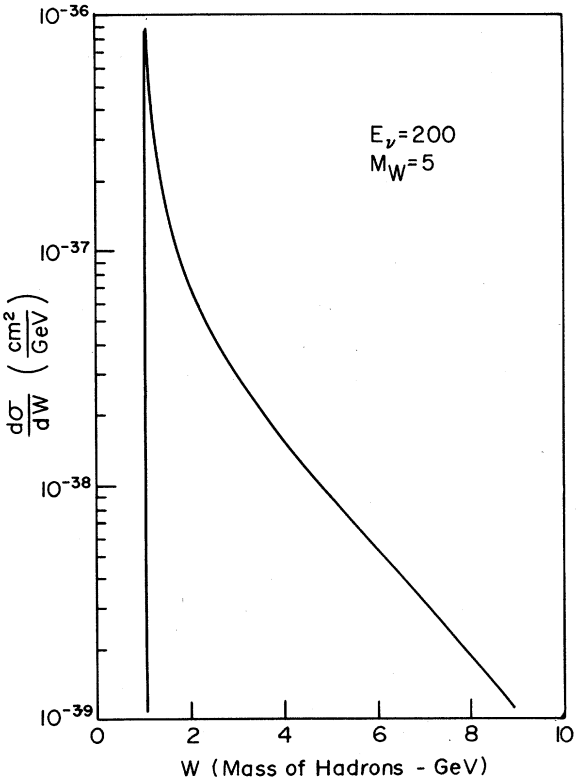

FIG. 24. $d\sigma/dW$ in cm^2/GeV versus W (the mass of the hadrons in GeV) for the inelastic scattering process.

(calculated according to the method in I) for the same parameters $M_W = 5$, $E_1 = 200$, and $\kappa = 0$. It is seen there that the cross section is strongly peaked in the smaller-W region. Hence, the channels with masses close to the proton are the most important. This is consistent, then, with the similarity of the inelastic spectra with the elastic spectra. It is interesting that the cross section for all of these inelastic channels comes mostly from the low-energy channels. (See Fig. 25 which was obtained by "binning" during the integrations of the earlier calculations.) It should be noted that the aforementioned similarity of the spectra is not affected by changing our fit in (7.4) to, for example, the drastic choice $F(\omega) = 0.3$.

It follows that we can expect the polarization of the W to be left handed since it again goes straight ahead with all of the energy and because the small W values are preferred. (We have not explicitly carried out the polarization calculation for these inelastic channels, but we refer the reader to the remarks in Sec. V.) Notice that this allows the decay spectra to be estimated according to the remarks of Sec. VI.

VIII. DISCUSSION AND CONCLUSIONS

The qualitative nature of our "elastic" incoherent and coherent results is certainly in agreement with general expectations. Knowing that we are limited to the region near the smallest allowed momentum transfer, a large ratio for M_W/μ means that the W will obtain nearly all of the neutrino's energy in the laboratory. This in turn implies that the W cannot be produced at a wide angle with respect to the incident neutrino beam since it has almost all of the momentum. The small deflections for the prompt muons are more surprising, but again understandable since at minimum q^2, the W^+ and μ^- must travel in the same laboratory direction.

The W^+ polarization continues to be predominantly left handed at the higher energies that we considered – this "following the neutrino helicity sense" was first discussed by Bell and Veltman.[8] We do see the necessarily larger angles of scattering for μ^- than for W^+ in accord with the discussion given in Ref. 8.

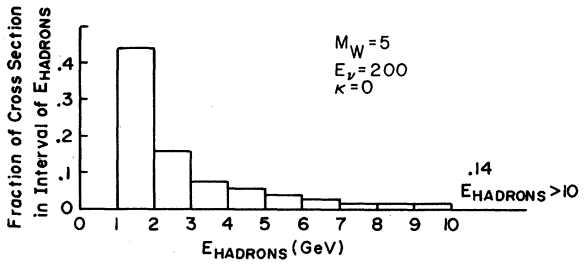

FIG. 25. Fraction of cross section in the interval of hadron energy versus the hadron energy.

We have seen that the breakup of the proton into deep-inelastic channels produces spectra for the μ^- and W^+ quite similar to that for the "elastic" case. It was important to ascertain the difference, if any, since the deep-inelastic cross section is comparable to the elastic cross section. Thus, the novel method proposed by Cline, Mann, and Rubbia[6] for the detection of W's by their hadron decays remains applicable to those W's produced inelastically. (We should note that Ref. 6 also contains some of our results in a slightly different "contour" form, where the contours have been inadvertently labeled in $M_W = 1$ units.) The point is that for all of our cases, the average momentum transfer across the ν_μ-μ^- line is much smaller in the W-boson production than in the deep-inelastic nucleon breakup in the absence of W-boson production, a result of the small average angles and energies seen for μ^-. In the notation of Ref. 6, subsequent more detailed calculations carried out by us have indicated that about one third of the cross section is inside of the area $x < 0.03$, $y > 0.85$. This does not seem to change the results too much, because the important deep-inelastic channels had been heretofore neglected. However a more detailed analysis is in progress and will be published later.

By concentrating on the leptonic decay (1.3), we have made the implicit assumption that its branching ratio is non-negligible. This is consistent with specific hadronic decay calculations[21] and, moreover, seems to be consistent with a recent estimate of the total hadronic decay branching ratio.[22] On the basis of these calculations, the branching ratio for (1.3) should be anywhere from 10% to 30% [note that other lepton decays (e.g., $e^+ + \nu_e$) have comparable branching ratios].

The calculations for the antineutrino reaction (less favorable experimentally)

$$\bar{\nu}_\mu + Z \to Z + \mu^+ + W^-$$

parallel to the ones performed here would give identical results for the W^- and μ^+ spectra. However, now the W^- is expected to be right handed with a corresponding $(1 - \cos\theta^*)^2$ μ^--decay angular distribution in the rest frame of the W^-. This last result follows from CP invariance.

In general, we have neglected μ^2 terms in the traces (evaluated using Veltman's algebraic computer program). The error in doing so was seen to be of the order of (1–2)% by explicitly including these terms in typical cases. These corrections are consistent with those seen in the total cross sections.[23] We would like to emphasize that all of our differential cross sections, polarization calculations, and decay distributions were checked by

comparing the integrated results with the calculations in I. We can thus give an estimate of the accuracy in our figures and in Table II as a result of the total cross-section checks. For the histogram heights the errors are on the order of 4%, 10%, and 6% for the elastic, decay, and inelastic contributions, respectively. The errors in Table II are on the order of 3%. The coherent calculations are more accurate than these errors would indicate. Because our total cross sections were on the low side by the amounts indicated by the error estimate above, the energy and angular distribution curves are probably low by the same amount.

We have not taken into account the Fermi motion of the nucleons in our incoherent calculation. This effect[24] is significant only near threshold where the total cross section is very small anyway. The exclusion-principle suppression of small momentum transfers was also neglected in performing the incoherent computations presented here. However, simulating this effect by cutting off the form factors[25] produced only an over-all reduction in the differential cross section with little qualitative change. The reduction percentage can be estimated by the total cross-section reduction shown in I, noting that the histograms given as percentages are little changed.

A final remark is that a lower limit of 5 GeV/c^2 for M_W was recently estimated[26] by considering the absence of spurious muons from the cosmic-ray neutrino flux interactions with the earth. This estimate relied on an assumption about the average prompt-muon energy in the reaction (1.1). Namely, it was assumed that this average energy was about 50% of the incident neutrino energy. According to our results, this is quite incorrect; a much lower average prompt-muon energy has been seen for both elastic and inelastic modes. A more accurate lower limit would seem to be substantially below the stated 5 GeV/c^2. In fact, we have calculated the average energy for the cases of interest in cosmic-ray analysis and our results can be found in the work of Chen *et al.*[27] They find, indeed, that the lower limit is reduced to 2.9 GeV/c^2.

ACKNOWLEDGMENTS

We thank C. N. Yang for introducing us to this general problem. We are grateful for discussions with D. Frisch and A. K. Mann concerning the experimental situation and with R. L. Schult concerning the phase-space limits for three-particle final states. It is our pleasure to be able to thank R. F. Peierls and Brookhaven National Laboratory for hospitality during the course of this work.

---

*Work performed, in part, under the auspices of the U. S. Atomic Energy Commission.

†Present address.

[1]R. W. Brown and J. Smith, Phys. Rev. D 3, 207 (1971). This paper includes a rather complete list of references for the previous total cross section calculations and also a brief summary of the experimental status of the W.

[2]R. W. Brown, A. K. Mann, and J. Smith, Phys. Rev. Letters 25, 257 (1970).

[3]F. A. Berends and G. B. West, Phys. Rev. D 1, 122 (1970); 2, 1354(E) (1970); 3, 262 (1971).

[4]J. Reiff, Nucl. Phys. B23, 387 (1970).

[5]K. Fujikawa, thesis, Princeton University, 1970 (unpublished). J. Løvseth and M. Radomski, Phys. Rev. D 3, 2686 (1971).

[6]D. Cline, A. K. Mann, and C. Rubbia, Phys. Rev. Letters 25, 1309 (1970). The reader must be informed that the contours in Fig. 1 in this paper are labeled in $M_W = 1$ units. In a recent paper T. D. Lee [Phys. Rev. Letters 25, 1144 (1970)] proposed that a spin-zero W boson decaying into hadrons may be the most important decay mode of a spin-1 W boson.

[7]T. D. Lee, P. Markstein, and C. N. Yang, Phys. Rev. Letters 7, 429 (1961). More prompt-μ energy distributions can be found for these energies and masses in the articles by M. Veltman, in Proceedings of the International Conference on Fundamental Aspects of Weak Interactions, Brookhaven National Laboratory Report No. 837, 1963 (unpublished), p. 160 and CERN Lecture Notes 6397, 1963, (unpublished), p. 21.

[8]J. S. Bell and M. Veltman, Phys. Letters 5, 151 (1963). Note that these authors have employed a left-handed polarization basis.

[9]H. Überall, Phys. Rev. 133, B444 (1964).

[10]Our basic notation and conventions are those of J. D. Bjorken and S. D. Drell, *Relativistic Quantum Mechanics* (McGraw-Hill, New York, 1964); J. D. Bjorken and S. D. Drell, *Relativistic Quantum Fields* (McGraw-Hill, New York, 1965). In particular, $\hbar = c = 1$, $\alpha = e^2/4\pi$, and $\not{p} = \gamma^\mu p_\mu$.

[11]See I for the interaction Lagrangian and other details. However, $g_W^2 = (\frac{1}{2})^{1/2} G M_W^2$, where $G \simeq 10^{-5}/M_p^2$ is the Fermi coupling constant for the weak vector current.

[12]The most conservative approach would be to assume that the W boson, if it exists, has normal properties, i.e., no anomalous magnetic dipole or electric quadrupole moments. We have gone one step further by including an anomalous magnetic moment, but have neglected the quadrupole degree of freedom. Hence the dipole and quadrupole moments are given by $\mu_W = (e/2M_W) \times (1+\kappa)$, $Q = -(e/M^2)\kappa$.

[13]D. H. Coward *et al.*, Phys. Rev. Letters 20, 292 (1968); J. Litt *et al.*, Phys. Letters 31B, 40 (1970); W. Bartel *et al.*, *ibid.* 30B, 285 (1969); The possibility that scaling breaks down at larger momentum transfers [W. Bartel *et al.*, Phys. Letters 33B, 245 (1970)] has little effect on our results. The further possibility that $G_E(\text{neutron}) \simeq \tau G_M(\text{neutron})$ would only serve to increase the total neutron cross sections by about 10%, or less.

[14]H. H. Chen, Nuovo Cimento 69, A585 (1970).
[15]R. Burns *et al.*, Phys. Rev. Letters 15, 42 (1965); G. Bernardini *et al.*, Nuovo Cimento 38, 608 (1965). See I for additional references.
[16]This trace as well as other intermediate results implicit in our work can be obtained upon request.
[17]M. E. Rose, *Elementary Theory of Angular Momentum* (Wiley, New York, 1957).
[18]H. H. Chen, Phys. Rev. D 1, 3197 (1970). See also Refs. 1, 4, and 14.
[19]E. D. Bloom *et al.*, Phys. Rev. Letters 23, 930 (1969); M. Breidenbach *et al.*, *ibid.* 23, 935 (1969).
[20]W. Albrecht *et al.*, Nucl. Phys. B13, 1 (1969).
[21]R. E. Marshak, Riazuddin, and C. P. Ryan, *Theory of Weak Interactions in Particle Physics* (Wiley, New York, 1969), Chap. 7.
[22]L.-F. Li and E. A. Paschos, Phys. Rev. D 3, 1178 (1971). We thank Dr. Paschos for discussions concerning this calculation.
[23]See footnote 42 in I.
[24]G. von Gehlen, Nuovo Cimento 30, 859 (1963).
[25]J. S. Bell and M. Veltman, Phys. Letters 5, 94 (1963).
[26]R. Cowsik and Y. Pal, in Proceedings of the Eleventh International Conference on Cosmic Rays, Budapest, 1969 (unpublished).
[27]H. H. Chen, W. R. Kropp, H. W. Sobel, and F. Reines, Phys. Rev. D 4, 99 (1971).

PHYSICAL REVIEW D VOLUME 4, NUMBER 3 1 AUGUST 1971

Antibaryon-Baryon Scattering Problem*

Richard M. Weiner
Department of Physics, Indiana University, Bloomington, Indiana 47401
(Received 22 February 1971)

The implications of the failure of duality in $\bar{B}B$ scattering are discussed in the framework of a quark model in which all quarks of the target interact simultaneously with all quarks in the projectile through two-body quark-antiquark interactions. It is assumed that the peculiarity of $\bar{B}B$ interactions, which at the particle level manifests itself through annihilation channels, is due to the strong $q\bar{q}$ interaction at the quark level which inhibits the presence of nonactive quarks (spectators) in the scattering process. This leads to the replacement of the additivity approach of quark amplitudes by factorization of quark amplitudes. Factorization of quark amplitudes implies, in general, nonfactorization of particle amplitudes and appearance of effects similar to cuts (dips versus peaks in the forward direction) due to the simultaneous exchange of natural and unnatural parity at the quark level. Exchange of exotic quantum numbers appears as a natural consequence of the model, without assuming the existence of exotic particles. It is, however, inhibited by the smallness of charge- and strangeness-exchange cross sections. This model should apply both for large- and small-angle scattering, the difference in these two regions manifesting itself only through different relations between the helicity amplitudes at the quark level. Predictions are made for quasielastic $\bar{B}B$ scattering at small and large momentum transfer. For the reactions where data exist, the agreement between the relations predicted by the model and experiment is satisfactory.

I. INTRODUCTION: DUALITY, $\bar{B}B$ SCATTERING, AND EXOTIC STATES

The assumptions of (i) the nonexistence of exotic states of first or second kind,[1] and (ii) duality have led to remarkable results for MB scattering[2] (M and B represent a meson and baryon, respectively), constituting the starting point for many interesting developments in hadron phenomenology. However, it was soon realized that antibaryon-baryon scattering represented a singular case with respect to the compatibility between duality and nonexotic states, giving rise to a series of puzzles.

Indeed, Lipkin[3] has pointed out that hypotheses (i) and (ii) lead, e.g., to such paradoxes as the vanishing of the $\bar{\Delta}\Delta$ scattering amplitude. Another failure of duality and nonexotic states in $\bar{B}B$ scattering can be visualized in quite a simple way by contemplating duality quark diagrams.[4,5] While for MM and MB scattering the drawing of such diagrams is possible without invoking exotic states, for antibaryon-baryon scattering the consideration of exotic quantum numbers is unavoidable at least in one channel. Finally, the exchange degeneracy, which is a consequence of (i) and (ii), does not work in $\bar{B}B$ scattering. This was shown by Rosner[6] in connection with the s dependence of $\bar{B}B$ scattering amplitudes and is supported also by the recent experimental data of the CERN $\bar{p}p \to \bar{Y}^*Y$ experiment.[7]

The most obvious way to get out of this puzzling situation is to assume that either assumption (i) or assumption (ii) does not hold for $\bar{B}B$ scattering.

The first kind of approach has been chosen by